

Hillslope Hydrology and Geomorphology: Chemical Erosion and  
Implications for Hillslope Evolution

By

Eli Louis Schwat

Senior Thesis

Submitted to the Faculty of the

College of Arts and Science of Vanderbilt University

in partial fulfillment of the requirements

for the degree of

BACHELOR OF ARTS WITH HONORS

in

Earth and Environmental Sciences

April, 2018

Nashville, Tennessee

Approved by:

---

David Jon Furbish, PhD

---

Date:

---

Dan Morgan, PhD

---

Date:

---

Departmental Honors Director: Lily Claiborne, PhD

---

Date:

## Acknowledgments

I would like to thank Dr. David Furbish for being an inspiration in both my academic and personal life. Over the past four years, Dr. Furbish has introduced me to a world of science and mathematics that was previously unknown and inaccessible to me. He has given me direction in my studies and also in my personal career goals. My love for challenging scientific and mathematical problems continues to grow and I attribute that continuing growth to my experiences in many of Dr. Furbish's classes as well my experience performing research under his watch. Dr. Furbish has always been kind, honest, and, best of all, careful to give me the academic freedom to explore the depths of my own mind.

I owe a great deal to Dr. George Hornberger, Dr. Neil Kelley, and Dr. Lily Claiborne. Dr. Hornberger has inspired me towards the fields of hydrology and fluid mechanics. Dr. Kelley has provided me direction in being an all around good scientist and writer. Dr. Claiborne has been an excellent undergraduate advisor, providing me advice when needed, pushing me towards multiple research opportunities, and also giving me freedom within the major.

Thank you also to Dr. Morgan for his wealth of geomorphological knowledge and offering me detailed suggestions and to Dr. Marcelo Disconzi for spending many hours at the chalkboard with me.

Thank you to my friends who do not complain (too much) when I talk endlessly about the mysteries of rainwater in the subsurface and the incredible importance of soil creeping down hillslopes. Thank you lastly to my parents who have always supported me in all of my academic endeavors.

# Table of Contents

<b>List of Figures</b>	<b>4</b>
<b>List of Tables</b>	<b>5</b>
<b>Abstract</b>	<b>6</b>
<b>1 Introduction</b>	<b>7</b>
<b>2 Conceptual Model</b>	<b>10</b>
2.1 Hillslope Definition . . . . .	10
2.2 Hillslope Form: Profile Concavity . . . . .	11
2.3 Hillslope Form: Planform and the Quasi Two-Dimensional Framework . . . . .	13
2.4 Nine Hillslope Forms . . . . .	15
<b>3 Perched Water Table Flow</b>	<b>17</b>
3.1 Kinematic Wave Approximation for Perched Water Table Flow . . . . .	17
3.2 Analytical Solutions to the Kinematic Wave Equation . . . . .	19
3.3 Accuracy of the Kinematic Wave Approximation . . . . .	21
3.4 Simulation Methodology . . . . .	22
<b>4 Chemical Denudation Rates Due to Perched Water Table Flow</b>	<b>23</b>
4.1 Net Exposure Time . . . . .	23
4.2 Mineral Dissolution Model . . . . .	23
4.3 Annual Storm Ensemble . . . . .	25
4.4 Dissolution Rates and Chemical Denudation Rates . . . . .	26
4.5 Simulation Methodology . . . . .	29
<b>5 Hillslope Evolution</b>	<b>30</b>
5.1 Soil Diffusion in the Quasi Two-Dimensional Framework . . . . .	30
5.2 Hillslope Mass Balance Equation . . . . .	31
5.3 Numerical Hillslope Model . . . . .	32
5.4 Initial Conditions . . . . .	33
5.5 Boundary Conditions . . . . .	33
5.6 Hillslope Simulation Parameters . . . . .	34
5.7 Calculating Denudation Ratios . . . . .	34
5.8 Simulation Methodology . . . . .	35
<b>6 Results and Discussion</b>	<b>37</b>
6.1 Perched Water Table Flow and Chemical Denudation . . . . .	37
6.2 Hillslope Evolution Simulations . . . . .	41
6.2.1 Diffusion Only Simulations . . . . .	41
6.2.2 Varying the Strength of Chemical Erosion . . . . .	42
6.2.3 Varying Convergence Rate . . . . .	45
6.2.4 Varying Rainstorm Frequency and Intensity . . . . .	48
6.2.5 Varying Diffusivity, Hillslope Evolution Over Longer Timescales . . . . .	49
6.3 Addressing Assumptions . . . . .	50
<b>7 Conclusion: Implications for Hillslope Evolution</b>	<b>54</b>

<b>8</b>	<b>References</b>	<b>56</b>
<b>9</b>	<b>Supplemental Material</b>	<b>59</b>
9.1	Method of Characteristics for Perched Water Table Flow . . . . .	59
9.1.1	Analytical Solutions to the Kinematic Wave Equation, Planar Hillslope . . . . .	60
9.1.2	Analytical Solutions to the Kinematic Wave Equation, Parabolic Hillslope . . . . .	63
9.1.3	Calculating the Rise and Decay of a Perched Water Table . . . . .	64
9.2	Hillslope Evolution Simulations . . . . .	66

## List of Figures

1	Two-dimensional hillslope undergoing soil diffusion, From Mudd and Furbish (2004)	8
2	Definition hillslope	11
3	Three characteristic hillslope concavity profiles	12
4	Three characteristic hillslope planforms	15
5	Nine hillslope forms, adapted from Troch et al. (2002)	16
6	Figure demonstrating the method of characteristics for the kinematic wave approximation, adapted from Troch et al. (2002)	20
7	Water table draining on nine hillslopes	38
8	Exposure time on nine hillslopes after a single rainstorm	39
9	Annual chemical denudation on nine hillslopes	40
10	Annual chemical denudation on convex hillslopes with linear fits	41
11	Hillslope evolution with soil diffusion only, convex hillslope	42
12	Hillslope evolution with soil diffusion and chemical erosion, varying strength of chemical erosion, convex hillslope	43
13	Hillslope evolution with soil diffusion and chemical erosion, varying strength of chemical erosion, planar hillslope	44
14	Hillslope evolution with soil diffusion and chemical erosion, varying convergence rate, convex hillslope	46
15	Hillslope evolution with soil diffusion and chemical erosion, varying convergence rate, concave hillslope	47
16	Hillslope evolution with soil diffusion and chemical erosion, varying rainstorm frequency and intensity, convex hillslope	49
17	Hillslope evolution with soil diffusion and chemical erosion, varying diffusivity over long timescales with low chemical erosion, convex hillslope	51
18	Hillslope evolution with soil diffusion only, planar hillslope	66
19	Hillslope evolution with soil diffusion only, concave hillslope	67
20	Hillslope evolution with soil diffusion and chemical erosion, varying strength of chemical erosion, concave hillslope	68
21	Hillslope evolution with soil diffusion and chemical erosion, varying climate, planar hillslope	69
22	Hillslope evolution with soil diffusion and chemical erosion, varying climate, concave hillslope	70
23	Hillslope evolution with soil diffusion and chemical erosion, varying convergence rate, planar hillslope	71
24	Hillslope evolution with soil diffusion and chemical erosion, varying diffusivity over long timescales with low chemical denudation rates, planar hillslope	72
25	Hillslope evolution with soil diffusion and chemical erosion, varying diffusivity over long timescales with low chemical denudation rates, concave hillslope	73

## List of Tables

1	Hillslope concavity parameters describing the three forms shown in Figure 3. . . . .	13
2	Hillslope planform parameters describing the three forms shown in Figure 4 . . . . .	14
3	Accuracy of the kinematic wave equation . . . . .	22
4	Parameters for the Chemical Denudation Function . . . . .	27
5	Hillslope Evolution Simulation Parameters . . . . .	34

## Abstract

Hillslope geomorphology has traditionally focused on the mechanical processes that create and move soil on soil-mantled hillslopes. The growth of critical zone sciences has broadened our understanding of the hydrological and chemical processes operating on hillslopes and has created an opportunity to broaden our understanding of land surface processes. Numerical simulations of hillslope evolution incorporating subsurface hydrologic flow and mineral dissolution suggest that chemical denudation may be an important factor in the development of varied hillslope topographies. By characterizing subsurface hydrologic flow on soil-mantled hillslopes with a fluid dynamical model, net chemical denudation as a function of distance from the hillslope crest can be estimated. Estimations of chemical denudation along with the linear diffusion model of soil creep form an original mass-balance model that simulates the evolution of two-dimensional hillslopes. The model simulates both mechanical-diffusive denudation and chemical denudation on hillslopes with convergent, divergent, and uniform planforms with convex parabolic, concave parabolic, and planar profiles. Diffusive processes smooth varied hillslope topography and chemical processes may introduce topographic variation. At low chemical denudation rates, diffusive processes dominate hillslope evolution and convergent and divergent hillslopes evolve similarly, suggesting that purely diffusive hillslope denudation acts stably, as previous studies have suggested. At high chemical denudation rates, chemical processes dominate and convergent and divergent hillslopes evolve differently due to the differences in the magnitude of convergent and divergent subsurface hydrologic flow and resultant chemical denudation. Chemical denudation is particularly sensitive to the convergence rate of the hillslope form; the greater the convergence of hillslope planform, the greater the net chemical denudation. This relationship suggests that chemical denudation may act as a positive feedback mechanism, in which increased chemical denudation on convergent hillslopes causes hillslopes to become more convergent, thereby increasing the magnitude and duration of subsurface flow over the hillslope and increasing chemical denudation further. Chemical denudation rates are also sensitive to climate, with increased rainstorm frequency increasing denudation rates due to the non-linear behavior of subsurface hydrologic flow. Over longer timescales, low chemical denudation rates may still introduce topographic variation where soil creep diffusivity is low.

# 1 Introduction

Hillslope geomorphologists have recognized for a long time the apparent ubiquity of soil-mantled, gently sloping hillslopes. These systems represent a steady conversion of bedrock to soil and a steady transport of soil to streams. Over the last century, hillslope studies have primarily focused on the mechanical transport of earth materials and the expression of this transport in topographic form. The seminal work of Culling (1960) on a theory of erosion explored a model for mechanical soil movement using a diffusion equation and many studies have since explored the mechanical means of hillslope evolution and have used increasingly complex mathematical models, including nonlinear diffusion (Roering, 1999) and non-local transport (Foufoula–Georgiou, 2010; Furbish and Haff, 2010; Furbish and Roering, 2013; Doane et al., 2018). Focusing exclusively on mechanical transport, however, ignores a whole suite of non-mechanical processes also acting on soil-mantled hillslopes. Recent developments in the broader geosciences have focused on the complex processes that occur within the critical zone, the section of the Earth’s crust extending from the deepest groundwater to the tops of the highest tree canopies. The critical zone is a multi-phase system involving bedrock, saprolite, soil, and water (Anderson et al., 2007; Dixon et al., 2009; Anderson and Anderson, 2010) and hillslope transport processes operate well within the domain of the critical zone. Perhaps examining geomorphology as a product of the many processes that act within the critical zone can provide unique insight into the formation of hillslope topographies.

As earth materials become physically mobile, they are exposed to chemical solutions composed of rainfall with dissolved gases and minerals. The layers of bedrock, saprolite, and soil beneath the land surface act as a feed-through reactor, in which chemical solutions flow, converting bedrock to soil, with saprolite often an intermediate phase, with the aid of mechanical processes (Anderson et al., 2007; Anderson and Anderson, 2010; Jin et al., 2010; Dixon and Riebe, 2014). Though many geomorphological studies consider only the impact of mechanical transport on hillslope evolution, research has suggested that half of all mass flux away from a hillslope may be due to chemical processes operating within the saprolite (Ferrier et al., 2010). A consideration of how non-mechanical transport processes influence hillslope evolution is a logical next step in seeking a more complete understanding of hillslope geomorphology.

Through a numerical stability analysis, Furbish and Fagherazzi (2001) determine that diffusive, mechanical soil transport has a stabilizing effect, keeping hillslopes smooth (Figure 1). In considering only the effects of mechanical soil transport on hillslope evolution, we must conclude that hillslopes should approach smooth conditions with diminished topographic variability. Although smooth hillslope forms exist, they are not the only forms observed in the field. Topographic variation perpendicular to the downslope direction (parallel to a main stem channel, as in Figure 1) is common; rarely if ever are extensive uniform surfaces encountered. A basic geomorphological question is thus raised: what processes contribute to the morphological diversity observed on hillslopes?

Perhaps recasting the question of hillslope geomorphology in terms of chemical processes can help us answer this question. We know of three studies that examine the relationship between chemical erosion and hillslope morphology. Mudd and Furbish (2004) explore how spatially uniform chemical denudation rates influence steady state hillslope geometries and discover that chemical denudation, along with linear soil diffusion, produces steady state hillslopes of a flatter parabolic form and, in some cases, convex-concave forms. Jin et al. (2010) focus on the geochemistry of hillslopes, looking at the distribution of mineral dissolution reaction fronts on hillslopes with different planforms. Jin and Brantley (2011) compare the geochemistry of soils in swale and planar transects and find that swale transects generally have thicker, wetter soils, the geochemistry of which indicate that soil accumulates in the swale transect. While geomorphologists have used both steady state and transient hillslope evolution simulations to understand

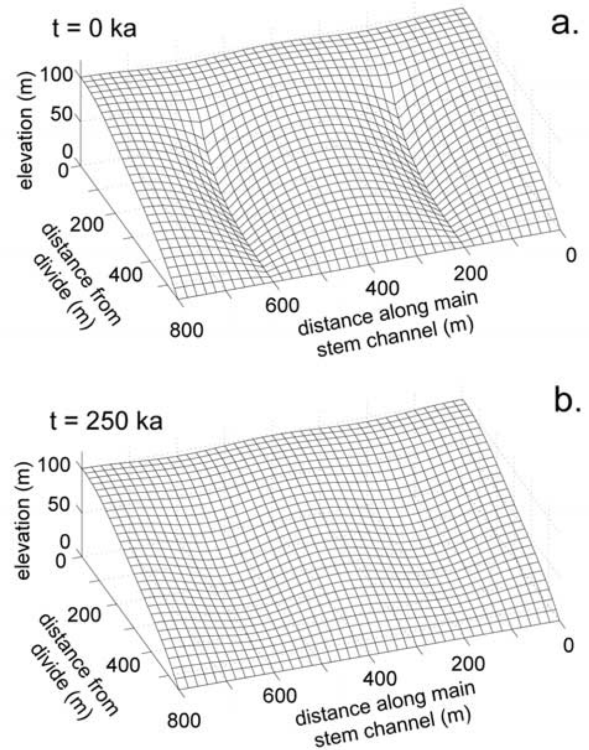


**Figure 1:** A two-dimensional hillslope subjected to soil diffusion evolving from a state of topographical variation at an initial state ( $t = 0$ , subplot a.) over 250,000 years ( $t = 250\text{ka}$ , subplot b.). It is evident from this simulation that diffusion contributes stability to hillslope form. Adapted from Mudd and Furbish (2004).

hillslope morphology as a product of erosive processes, we know of no studies that have simulated transient hillslope evolution while accounting for chemical erosion.

Because water is the solvent causing chemical erosion, we characterize the movement and residence time of water in the subsurface to calculate chemical erosion rates. In doing so, we encounter a challenging problem at the intersection of hydrology and hillslope geomorphology. Subsurface flow, which acts on short, day or week-long timescales, causes chemical erosion, which over long, geomorphic timescales of thousands of years, may influence hillslope morphology. In the following, we link the two timescales by modeling the dynamics of water in the subsurface and averaging the resultant geochemical processes over geomorphic timescales.

To explore whether chemical processes contribute a positive feedback effect to hillslope evolution, we examine how existing hillslope topography can influence chemical erosion and mechanical soil transport. For example, Figure 1a shows a hillslope with lowered sections. Figure 1b makes it apparent that linear soil diffusion removes the swales, as does the stability analysis of Furbish and Fagherazzi (2001). Perhaps, acting oppositely to soil diffusion, chemical erosion removes more mass from lowered sections, accentuating swale topography. It seems likely that the swales on the hillslope experience convergent hydrologic flow and perhaps extended exposure to rainfall solutions. Perhaps convergent flow in the swales causes preferential chemical erosion and mass-wasting within the swales and causes hillslope evolution to proceed under the influence of a positive feedback.

In what follows, we define a hillslope and the chemical and mechanical processes operating on it. We define nine distinct hillslope forms that represent unique topographies, such as those seen across the hillslope in Figure 1a, and which we expect may experience chemical and mechanical erosion of different magnitudes. We formulate a physics based model of subsurface, shallow storm flow, which we call perched water table flow, that can describe the unique subsurface fluid dynamics on each of the hillslope forms. We use the modeled fluid dynamics to estimate chemical erosion on the hillslopes, being careful to combine the hydrologic and geomorphic timescales. We then formulate a numerical model for hillslope evolution and run a series of simulations to explore how chemical and mechanical erosion influence hillslope evolution through time. After we present the simulations, we discuss what they imply about hillslope geomorphology and the possibility that chemical processes cause a positive feedback of denudation.

## 2 Conceptual Model

### 2.1 Hillslope Definition

In this study, a hillslope consists of a soil mantle that overlies a layer of saprolite, which in turn overlies bedrock (Figure 2). The soil mantle is physically mobile and subject to mechanical erosion and the saprolite is chemically mobile and subject to chemical erosion (Dixon and Riebe, 2014). Bedrock is also chemically mobile and, in fact, chemical dissolution is responsible for converting bedrock to the more weathered saprolite (Jin et al., 2010); however, we do not address this here. Mechanical erosion of the soil column is described with the linear diffusion model, which states that the downslope flux of soil is proportional to the local slope of the land surface (Culling, 1960; Dietrich, 2003; Anderson and Anderson, 2010). Chemical erosion of the saprolite is described as a downward lowering rate, which we approximate by accounting for the dissolution of minerals in the saprolite and the subsequent transport of the dissolved mass away from the hillslope.

The linear diffusion model of soil erosion is well defined in the literature (Culling, 1960, Furbush and Fagherazzi, 2001). Chemical denudation at the hillslope scale, however, is not. We formulate an original model with the following assumptions. Dissolution of saprolite material occurs when water is present in the subsurface.

Significant mineral dissolution only occurs in the upper layers of saprolite and is caused by the infiltration of water from above the soil-saprolite interface. In response to a rainstorm, water infiltrates through the soil column and a perched water table forms above the soil-saprolite interface (Scanlon et al., 2000) because the hydraulic conductivity of saprolite is much less than that of soil. Water beneath the perched water table simultaneously flows downslope atop the saprolite layer and infiltrates vertically downward into the saprolite. The perched water table rises above the soil-saprolite interface at the onset of a rainstorm, rises throughout the length of the rainstorm, and drains from the hillslope when the rainstorm ends. While the perched water table exists above the soil-saprolite interface, water flows into the saprolite and mineral dissolution occurs. When the water table drains below the soil-saprolite interface, water ceases to flow into the saprolite and any continuing mineral dissolution is negligible.

To describe both mechanical and chemical processes occurring on a hillslope, we need a mathematical description of hillslope geometry. We describe the profile concavity of the hillslope, how

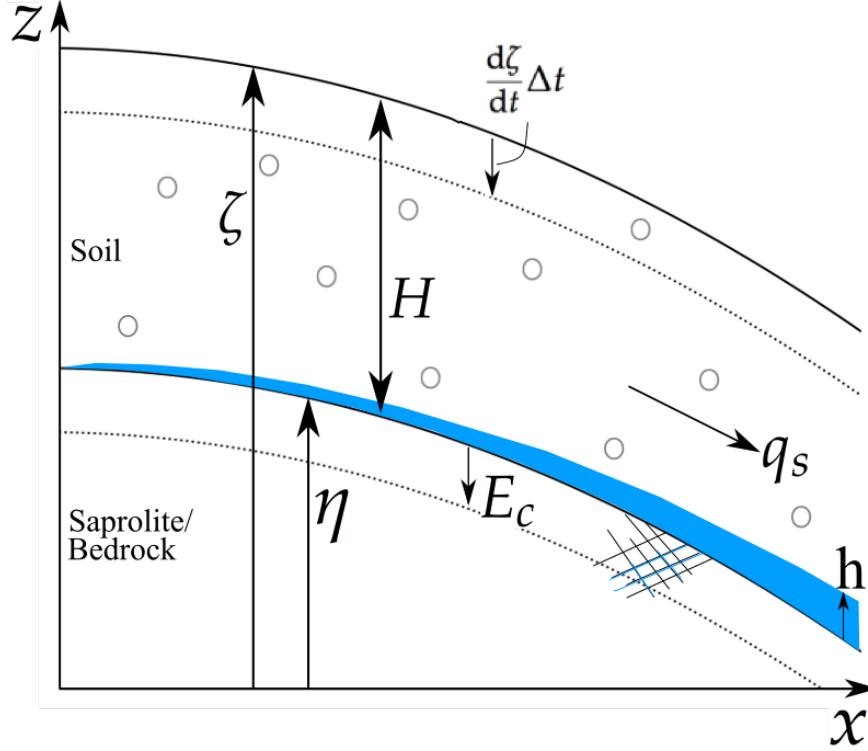


**Figure 2:** Definition hillslope showing the elevation of the soil-saprolite interface,  $\eta$ , the elevation of the land surface,  $\zeta$ , and the thickness of the soil mantle,  $H$ . Two erosive processes act on the hillslope: downslope soil diffusion,  $q_s$ , chemical erosion,  $E_c$ , caused by the perched water table, and  $h$ , the height of the perched water table above the soil-saprolite interface.

elevation varies between the crest and the bottom of the hillslope, and the planform, how elevation varies parallel to a stream channel positioned at the bottom of the hillslope. We place our hillslope in a Cartesian coordinate system, with the  $x$ -axis normal to and the  $z$ -axis parallel to the direction of gravity (Figure 2). The crest of the hillslope is at  $x = 0$  and the hillslope extends downwards in the positive  $x$  direction. The boundary at  $x = 0$  forms a no flux boundary; no water or soil enters the hillslope laterally, although water does enter from above. The bottom edge of the hillslope is at  $x = L$ , where we imagine a stream channel (Figure 1) that transports away all mass brought into it. Soil and water can only leave the hillslope from the bottom, at  $x = L$ .

## 2.2 Hillslope Form: Profile Concavity

Kirkby (1971) found that hillslopes generally take on three forms – convex, planar, and concave – depending on the transport processes operating on them. In their study of subsurface flow, Fan

and Bras (1998) use a second order polynomial of the form

$$\zeta(x) = \gamma + \beta x + \alpha x^2, \quad (1)$$

where  $\gamma$  is the height of the hillslope at the crest,  $\beta$  is the slope at the crest, and  $\alpha$  is the rate of change of slope with respect to  $x$ . Using this polynomial, we can define three hillslopes with profiles of distinct concavity as dictated by the work of Kirkby (1971) (Figure 3). On each of

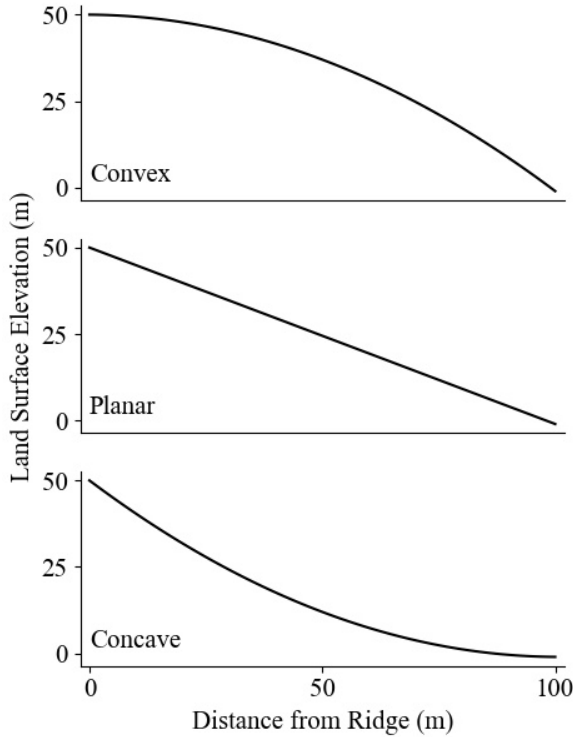


**Figure 3:** Profiles of the three characteristic hillslope forms convex, planar, and concave. The three forms are described mathematically by equation 1 and Table 1.

these hillslopes, we assume that the soil column thickness,  $H$ , is on the order of a meter and is spatially uniform such that the soil-saprolite interface, where the perched water table forms, is a downwards translation of the land surface,

$$\eta(x) = \gamma - H + \beta x + \alpha x^2. \quad (2)$$

**Table 1:** Hillslope concavity parameters describing the three forms shown in Figure 3.

Hillslope Concavity	$\gamma$	$\beta$	$\alpha$
Concave	50	-0.01	0.005
Planar	50	-0.51	0
Convex	50	-1.01	-0.005

We use the geometry of the soil-saprolite interface to explore the dynamics of perched water table flow (and chemical erosion) and we use the geometry of the land surface (or, equivalently, soil surface) to describe mechanical soil transport with the linear diffusion model.

We explicitly define three hillslope concavity profiles, which we use to calculate perched water table dynamics and as initial conditions for hillslope evolution simulations, in Table 1. All three hillslope profiles are 100 meters long ( $L = 100$ ). The ridge of each hillslope is at  $x = 0$  and is 50 meters high ( $\gamma = 50$ ). It is worth noting that  $\gamma$  has no impact on hydrology or geomorphology and serves only as a reference datum. Note that the parameters in Table 1 are chosen such that the concave and convex hillslopes contain the same range of slopes, the planar hillslope has the mean slope of the other two, and the steepest angle of any of the slopes is approximately  $45^\circ$ . These geometries are consistent with those of soil mantled hillslopes found in humid climates, such as the hills of the Appalachians and the eastern United States.

### 2.3 Hillslope Form: Planform and the Quasi Two-Dimensional Framework

To examine how hillslopes evolve in response to both mechanical and chemical erosion, we wish to understand how existing hillslope topography influences erosive processes. The profile concavity (topographic variation in the  $x$  direction) is an important starting point for doing so, but we wish to define two-dimensional hillslope forms with complex topographies, such as those shown in Figure 1a. To define such forms, we must describe the planform of the hillslope, how  $\zeta$  varies with  $y$ , how the land surface varies parallel to the stream channel. Describing hillslope planform allows us to compare the differences in the evolution of convergent and divergent hillslopes and thus allows us to explore whether a positive feedback mechanism may exist due to chemical erosion.

To make the study of two-dimensional hillslope geometries and the fluid flow that occurs on them mathematically tractable, we collapse the geometry of a two-dimensional hillslope into a one-dimensional equation. To do so, we define a contour width function,  $b(x)$ , which describes

**Table 2:** Hillslope planform parameters describing the three forms shown in Figure 4

Hillslope Planform	$b_0$	$c$
Convergent	30	-0.2
Uniform	20	0
Divergent	10	0.2

the width between two flow lines (lines following the steepest downslope direction) as a function of  $x$ . This approach essentially assumes that there are two impermeable flow lines bounding transport of any material such that we limit the area over which we account for soil and water. It also allows us to describe a hillslope as convergent (as within the swales of Figure 1a) or divergent (as in between the swales).

Fan and Bras (1998) demonstrate how a description of water on a two-dimensional hillslope can be collapsed into a one-dimensional hillslope water storage profile (Troch et al., 2002). Their method integrates the total surface area of a hillslope between two contour lines using contour data found in the field. We choose to use a linear contour width function when conserving mass (both soil and water) and, by including the contour width function in our equations of conservation, we may approximate the average profile of a perched water table and the average land surface profile within our bounded area.

Our linear contour width function takes the form

$$b(x) = b_0 + cx, \quad (3)$$

where  $b_0$  is the contour width at the ridge and  $c$  describes a convergence factor, the rate at which flow lines converge (or diverge) in the downslope direction. The linear contour width function can describe three general planforms that hillslopes may take: convergent, uniform, and divergent. A hillslope is convergent if flow lines converge downslope ( $c < 0$ ), divergent if flow lines diverge downslope ( $c > 0$ ), and uniform if flow lines are parallel ( $c = 0$ ) (Figure 4). Thus, we can modulate hillslope geometry from convergent to uniform to divergent with the adjustment of a single parameter,  $c$ . Note that, by definition, flow lines do not intersect.

An overhead map view of our three planforms (Figure 4) shows that the boundaries determined by the contour width function form symmetrical trapezoids for the convergent and di-

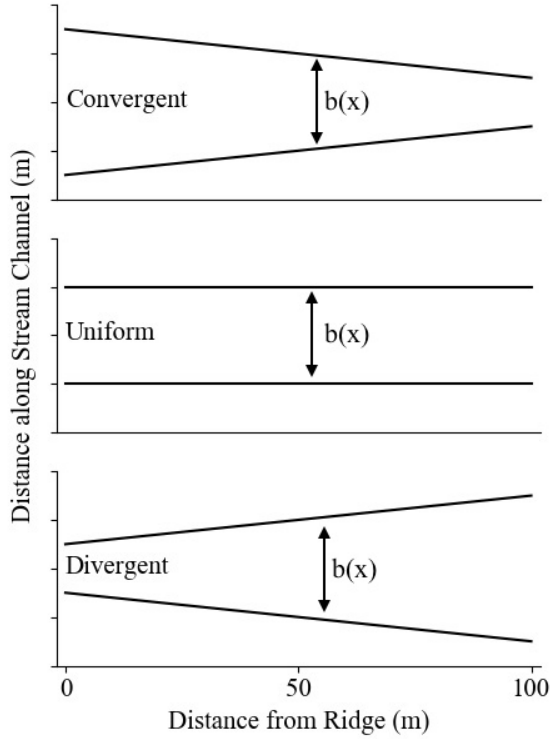


**Figure 4:** Contour width functions describing the three characteristic hillslope planforms: convergent, uniform, and divergent. Contour width is described by equation 3.

vergent hillslopes and a rectangle for the uniform hillslope (Figure 4). For the remainder of our analysis, we keep the areas of the trapezoids and rectangle constant. As Figure 4 demonstrates, each hillslope has equal width at  $L/2$  ( $b(L/2)$  is equal on all hillslopes). The convergent and divergent hillslopes have equal convergence factors,  $c$ , of opposite sign. The total surface area of each characteristic hillslope is equal, the net rainfall falling on each hillslope during a storm is equal, and thus evolution of hillslopes with different planforms may be compared directly.

## 2.4 Nine Hillslope Forms

Imposing each of the three planforms over each of the three profile concavities renders nine distinct hillslope geometries that we expect exhibit distinct mechanically and chemically erosive behavior. Troch et al. (2002) use a bivariate quadratic function to describe the three-dimensional geometry of nine hillslopes. Although the hillslopes defined by Troch et al. (2002) are conic sections, the nine hillslopes we model by imposing the linear contour width function (equation 3)

on the quadratic profile equation (equation 1) are of the same basic character as those of Troch et al (2002): (1) concave convergent, (2) concave uniform, (3) concave divergent, (4) planar convergent, (5) planar uniform, (6) planar divergent, (7) convex convergent, (8) convex uniform, and (9) convex divergent (Figure 5). We can now use our nine hillslope forms to explore the dynamics of perched water table flow, chemical erosion, and mechanical transport processes.

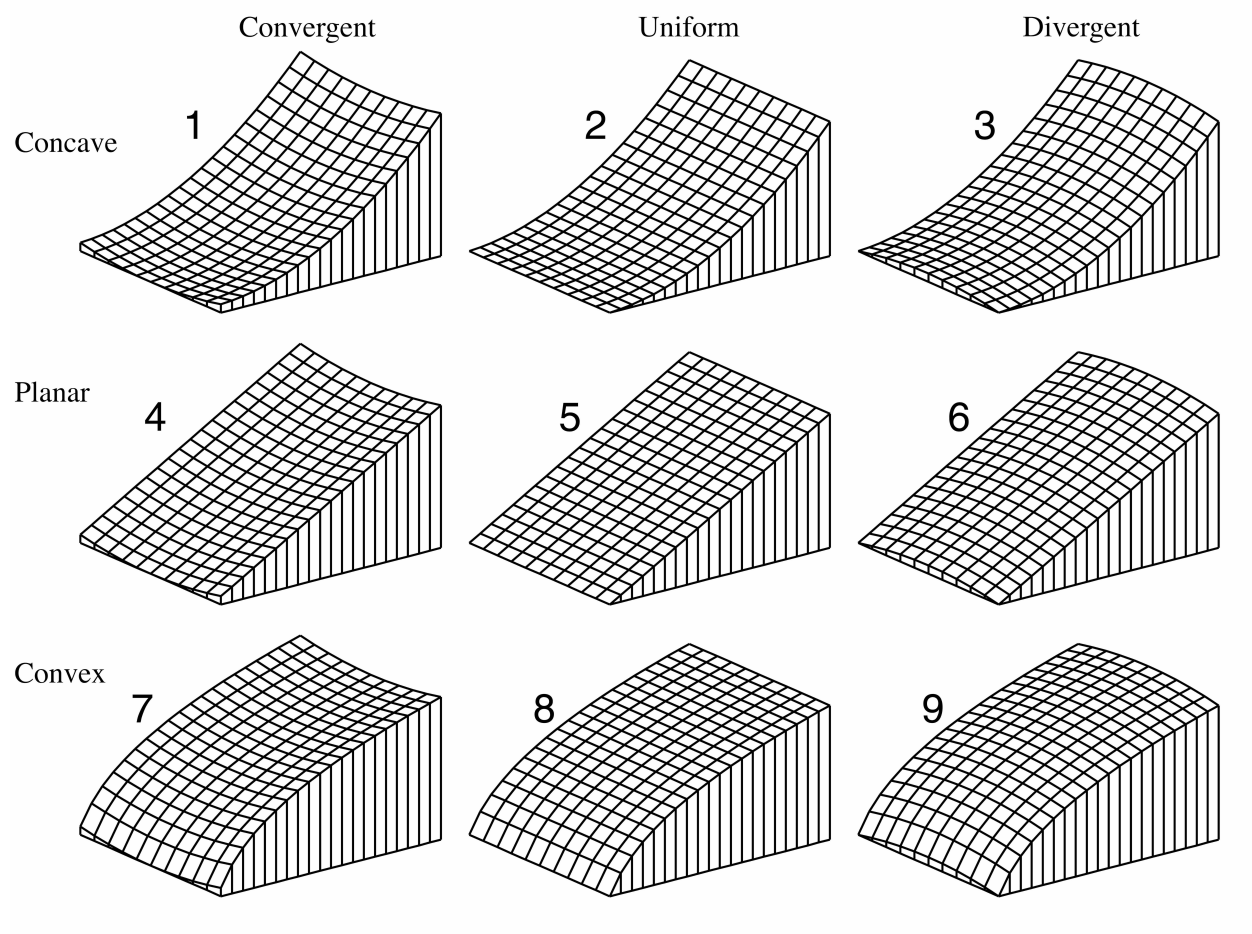


**Figure 5:** Nine geometries representing hillslope forms at the scale of a single hollow or ridge. The nine forms exhibit all combinations of planform (convergent, uniform, divergent) and profile concavity (convex, planar, concave). Note that the figures of Troch et al. (2002) figures demonstrate perfect conic sections while our hillslopes are better described as trapezoids and rectangles imposed upon parabolic surfaces. The hillslopes are numbered: (1) concave convergent, (2) concave uniform, (3) concave divergent, (4) planar convergent, (5) planar uniform, (6) planar divergent, (7) convex convergent, (8) convex uniform, and (9) convex divergent. Adapted from Troch et al. (2002).

### 3 Perched Water Table Flow

To estimate chemical erosion we first must describe the dynamics of subsurface flow. Specifically, we want to calculate the height of a water table perched above the soil-saprolite interface as a function of space,  $x$ , and time,  $t$ , in response to a single rainstorm. The perched water table will rise as it rains and lower as it drains after a rainstorm ends. The kinematic wave approximation allows us to analytically calculate the dynamics of a perched water table.

#### 3.1 Kinematic Wave Approximation for Perched Water Table Flow

Fluid flow on hillslopes in response to storms has been studied extensively in the fields of fluid dynamics and hydrology (Henderson and Wooding, 1964; Dunne and Leopold, 1978; Bevin, 1981; Giraldez and Woolhiser, 1996; Fan and Bras, 1998; Scanlon et al., 2000; Troch et al., 2002). Flow on a one-dimensional sloping hillslope is often described with the Boussinesq equation, which, in its general form, has no analytical solutions (Troch et al., 2002). When the angle of the inclined surface is relatively large, the second-order diffusive term in the Boussinesq equation becomes negligible and the kinematic wave approximation, which essentially assumes that gravity is the only force acting on the fluid, becomes applicable (Henderson and Wooding, 1964; Bevin, 1981). The Boussinesq equation for a water table perched atop a permeable saprolite layer takes the form

$$\frac{\partial h}{\partial t} + \frac{\partial}{\partial x}(hq_x) = N \quad (4)$$

where  $h$  is the height of the perched water table above the soil-saprolite interface,  $q_x$  is flux of water in the positive  $x$  direction, and  $N$  is a combined source-sink term, which we define as a constant rainfall rate minus the infiltration rate of water into the saprolite layer, which is equal to the hydraulic conductivity of the saprolite (which we assume is spatially uniform). Assuming that the precipitation rate never comes close to reaching the infiltration capacity of the soil, the infiltration rate,  $N$ , into the soil and into the perched water table, is equal to the precipitation rate. This assumption indicates that no Hortonian overland flow occurs on our hillslope, which is a safe assumption for relatively humid, forested, soil-mantled environments (Dunne and Leopold, 1978). To conserve fluid mass in our quasi two-dimensional framework, we include the contour

width function,  $b(x)$ , in each term of equation 4,

$$\frac{\partial}{\partial t}(b(x)h) + \frac{\partial}{\partial x}(b(x)hq_x) = Nb(x). \quad (5)$$

The kinematic wave approximation assumes that flux of water,  $q_x$ , is directly proportional to the slope of the surface over which it flows,

$$q_x = -\frac{K_h}{\epsilon} \frac{d\eta}{dx} = K \frac{d\eta}{dx} \quad (6)$$

where  $K_h$  is hydraulic conductivity,  $\epsilon$  is drainable porosity of the soil, and  $\frac{d\eta}{dx}$  is the slope of the soil-saprolite interface, the surface atop which water beneath the perched water table flows (as defined previously). We define effective hydraulic conductivity  $K = K_h/\epsilon$  for simplicity in the upcoming mathematics and assume that it is spatially uniform. Noting that  $b(x)$  and  $K$  do not vary with time, letting  $b$  denote  $b(x)$ , and combining equations 5 and 6, we find

$$b \frac{\partial h}{\partial t} - K \frac{\partial}{\partial x} \left( b h \frac{d\eta}{dx} \right) = Nb. \quad (7)$$

Expanding the second term using the product rule and reorganizing the resulting equation, we find

$$\frac{\partial h}{\partial t} - K \frac{d\eta}{dx} \frac{\partial h}{\partial x} = N + Kh \frac{b \frac{d^2\eta}{dx^2} + \frac{db}{dx} \frac{d\eta}{dx}}{b}. \quad (8)$$

From equation 2,  $\frac{d\eta}{dx} = \beta + 2\alpha x$  and  $\frac{d^2\eta}{dx^2} = 2\alpha$ , and from equation 3,  $\frac{db}{dx} = c$ . Thus equation 8 can be rewritten

$$\frac{\partial h}{\partial t} - K(\beta + 2\alpha x) \frac{\partial h}{\partial x} = N + Kh \frac{c\beta + 4\alpha cx + 2\alpha b_0}{(b_0 + cx)}. \quad (9)$$

Equation 9 is a quasi-linear wave equation (Logan, 1987), a partial differential equation in the form of a wave equation with a source/sink term and a non-constant wave speed (the coefficient  $-K(\beta + 2\alpha x)$ ). If  $N$  is constant, i.e. if rainfall rate and saprolite hydraulic conductivity are constant, equation 9 can be solved with the method of characteristics, which splits the equation into two ordinary differential equations (Logan, 1987; Fan and Bras, 1998; Troch et al., 2002),

$$\frac{dx}{dt} = -K(\beta + 2\alpha x), \quad (10)$$

which describes a family of characteristic curves in the  $x$  -  $t$  plane, and

$$\frac{dh}{dx} = -\frac{N}{K(\beta + 2\alpha x)} - h(x, t) \frac{c\beta + 4\alpha cx + 2\alpha b_0}{(b_0 + cx)(\beta + 2\alpha x)}, \quad (11)$$

which describes how the perched water table propagates along these curves (Fan and Bras, 1998; Troch et al., 2002). Note that we have replaced  $h$  with  $h(x, t)$  to clarify the dependent and independent variables in the differential equation 11. For the planar hillslope, where  $\alpha = 0$ , the two equations simplify to

$$\frac{dx}{dt} = -\beta K, \quad (12)$$

and

$$\frac{dh}{dx} = -\frac{N}{\beta K} - h(x, t) \frac{c\beta}{\beta(b_0 + cx)}. \quad (13)$$

In deriving the analytical solutions for the rise and decay of a perched water table on a hillslope, we follow the examples of Fan and Bras (1998) and Troch et al. (2002). It is worth noting that our model differs from each of their models in two respects. We allow water to drain into the surface over which it flows (similar to Girdzey and Woolhiser, 1996) while Fan and Bras and Troch restrict fluid movement to downslope flow over an impermeable surface (i.e. bedrock). Our hillslope forms are also uniquely defined by the combination of constant convergence rates and planar/-parabolic hillslope forms.

### 3.2 Analytical Solutions to the Kinematic Wave Equation

For either the planar or parabolic case, the two ordinary differential equations can be solved such that we can calculate the geometry of the perched water table over the  $x$  domain  $x = [0, L]$ , on two time intervals: the rising limb, over which  $t = [0, T_R]$ , and the draining limb,  $t = [T_R, T_D + T_R]$ , where  $T_R$  is the length of a rainstorm and  $T_D$  is the length of time that drainage is allowed to propagate. During the rising limb  $N$  equals a constant rainfall rate minus the drainage rate (hydraulic conductivity of the saprolite) and during the draining limb  $N$  equals just the drainage rate (again, the hydraulic conductivity of the saprolite).

The essence of the method of characteristics is shown in Figure 6. The rising limb and falling limbs must be solved over two  $x$  domains, split at the value  $x_{crit}$ , which propagates in the positive

$x$ -direction with each step forward in time. For now, we simply present the solutions to equations 10 and 11 for perched water table flow on a parabolic hillslope. Solutions for both the parabolic and planar cases, along with a detailed treatment of the use of the method of characteristics to solve the quasi-linear wave equation 9, can be found in Section 9.

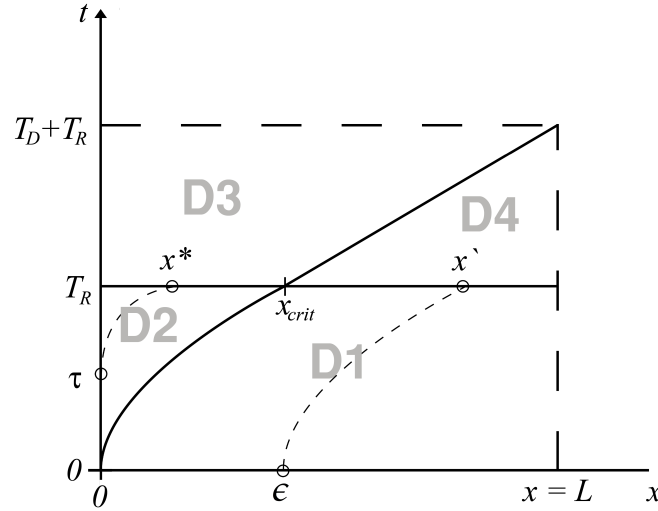


**Figure 6:** Figure demonstrating the method of characteristics for the kinematic wave approximation. The curve starting at  $(0,0)$  is the  $x - t$  path of the characteristic particle leaving from  $x = 0$ . We see that by the end of the rainstorm,  $T_R$ , the characteristic particle has not reached  $x = L$  and thus the water table has reached a state of partial equilibrium. Adapted from Troch et al. (2002)

The method of characteristics solves equation 9 over 4 domains. Domains 1 and 2 describe two sections of the perched water table immediately after a rainstorm of specified length and constant rainfall intensity. Domains 3 and 4 describe two sections of the water table after the rainstorm has ended and the water table has drained for a specified length of time. The solutions for perched water table flow on parabolic hillslopes are:

### Domain 1

$$x = \left( \epsilon + \frac{\beta}{\alpha} \right) e^{-\alpha kt} - \frac{\beta}{\alpha} \quad (14)$$

and

$$h(x) = \frac{N}{K(\beta + \alpha x)(b_0 + cx)} \left( b_0(\epsilon - x) + \frac{1}{2}c(\epsilon^2 - x^2) \right) \quad (15)$$

## Domain 2

$$x = \frac{B}{\alpha} \left( e^{\alpha K(\tau-t)} - 1 \right) \quad (16)$$

and

$$h(x) = \frac{-N(b_0x + \frac{1}{2}cx^2)}{K(\beta + \alpha x)(b_0 + cx)}. \quad (17)$$

## Domain 3

$$x = \left( x^* + \frac{\beta}{\alpha} \right) e^{\alpha K(T_R-t)} - \frac{\beta}{\alpha} \quad (18)$$

and

$$h(x) = \frac{N_D(b_0(x^* - x) + \frac{1}{2}c(x^{*2} - x^2))}{K(\beta + \alpha x)(b_0 + cx)} + h(x^*, T_R) \frac{(\beta + \alpha x^*)(b_0 + cx^*)}{K(\beta + \alpha x)(b_0 + cx)}. \quad (19)$$

## Domain 4

$$x = \left( x' + \frac{\beta}{\alpha} \right) e^{\alpha K(T_R-t)} - \frac{\beta}{\alpha} \quad (20)$$

and

$$h(x) = \frac{N_D(b_0(x' - x) + \frac{1}{2}c(x'^2 - x'^2))}{K(\beta + \alpha x)(b_0 + cx)} + h(x', T_R) \frac{(\beta + \alpha x')(b_0 + cx')}{K(\beta + \alpha x)(b_0 + cx)}. \quad (21)$$

### 3.3 Accuracy of the Kinematic Wave Approximation

Bevin (1981) examines in detail how the kinetic wave approximation compares to more complex formulations of fluid flow and determines that the kinematic wave method is acceptable for values of  $\lambda < 0.75$  where

$$\lambda = \frac{4N\cos\theta}{K\sin^2\theta}. \quad (22)$$

and  $\theta$  is the angle of incline. Bevin recognizes that the critical value 0.75 chosen for  $\lambda$  is somewhat arbitrary and, according to the results of both Bevin and Sloan and Moore (1984), it seems that differences in the magnitude of the perched water table, which is influenced by hillslope form, should still be described well by the kinematic wave approximation. Thus the inaccuracies inherent in the kinematic wave approximation are probably not significant enough to make any comparisons of potential chemical erosion due to subsurface flow on various hillslopes invalid.

Regardless, it is worth calculating the  $\lambda$  values associated with the parameters that we use in our simulations (Table 3). For the planar hillslope, where slope is 0.51 (Table 1), the  $\lambda$  value is

**Table 3:** Accuracy of the kinematic wave equation. The experiments of Bevin (1981) determine that the kinematic wave approximation is accurate where  $\lambda < 0.75$ .

N	K	Slope	$\theta$	$\lambda$
0.01 m hr <sup>-1</sup>	3.6 m hr <sup>-1</sup>			
		0.01	0.6°	111
		0.11	6.3°	0.913
		0.21	11.9°	0.247
		0.31	17.2°	0.110
		0.41	22.3°	0.0612
		0.51	27.0°	0.0381
		0.61	31.4°	0.0255
		0.71	35.4°	0.0180
		0.81	39.0°	0.0132
		0.91	42.3°	0.00992
		1.01	45.0°	0.00786

well within the limits of the accuracy threshold proposed by Bevin (1981). For the convex and concave hillslopes, for which slope varies from 0.01 to 1.01,  $\lambda$  is within the accuracy threshold for the majority of the hillslope. For the convex hillslopes, the kinematic wave approximation may be inaccurate for the upper 10 meters of the hillslope. For the concave hillslopes, the lower 10 meters.

### 3.4 Simulation Methodology

We use the analytical solutions to the kinematic wave approximation to characterize the drainage of the perched water table after a single storm. For the simulations presented in Section 6.1, we allow it to rain for three hours at one cm per hour and then turn the rain off. We then observe the drainage of the perched water table until it disappears beneath the soil-saprolite interface. The drainage rate into the saprolite is equal to the hydraulic conductivity of the saprolite, which we set to one tenth of the infiltration rate, one mm hr<sup>-1</sup> or  $2.78 \times 10^{-7}$  m s<sup>-1</sup>. This hydraulic conductivity is comparable to conductivities measured at the soil-saprolite interface in the field (Vepraskas et al., 1996). The simulation

## 4 Chemical Denudation Rates Due to Perched Water Table Flow

Our model uses subsurface hydrologic flow, which we can now describe analytically, as a proxy for chemical denudation on a hillslope. We wish now to formulate our model for chemical denudation as a result of subsurface flow. While a perched water table exists above the soil-saprolite interface, water continuously drains into the saprolite and chemical denudation occurs. If we know the length of time that water is infiltrating into the saprolite, then we can use mineral dissolution rates along with estimates of mineral surface area in the saprolite to calculate chemical denudation rates. Using the kinematic wave approximation for subsurface flow, we can calculate the amount of time that water is draining into the saprolite in response to a single rainstorm, which we call exposure time.

### 4.1 Net Exposure Time

When a perched water table exists above the soil-saprolite interface on a hillslope, at some positions  $x$ ,  $h(x) > 0$ . Wherever  $h(x) > 0$ , water is infiltrating into the saprolite. During a rainstorm and right when a rainstorm ends, the perched water table is above the soil-saprolite interface at all points on the hillslope; at  $T_R$ ,  $h(x) > 0$  for all  $x = [0, L]$ .

As the water table drains, the water table lowers below the soil-saprolite interface,  $h(x) < 0$ , at some positions  $x$ . Because solving for the position  $x$  where the water table crosses below the soil-saprolite interface as a function of  $t$  is mathematically daunting, we turn to a numerical solution. By observing the water table over the domain  $x = [0, L]$  at small time increments as drainage proceeds, we can numerically estimate the amount of time the water table is above the soil-saprolite interface,  $h(x) > 0$ , as a function of  $x$ . In addition to code we write in the Python language to solve the perched water table equations over the four domains, we write an algorithm that estimates the net exposure time of the soil-saprolite interface as a function of  $x$  after a given rainstorm.

### 4.2 Mineral Dissolution Model

Using the exposure time function described above, we can find the denudation rate of a one-dimensional soil-saprolite interface profile in units of length per time. We assume that as mineral

mass is lost due to dissolution in the presence of water, the density of saprolite remains constant, so the empty volume within the partially-dissolved saprolite is recovered, and the soil-saprolite interface is effectively lowered. This lowering seems realistic over geomorphic timescales, where chemical dissolution serves mainly to decrease saprolite density, priming it for biomechanical processes which break the upper saprolite layers apart and expose them to further erosion. We begin our calculation by noting that if the density of dissolving saprolite is kept constant, a change in saprolite volume is proportional to a change in saprolite mass,

$$\Delta V = \frac{\Delta m}{\rho}, \quad (23)$$

where  $V$  is saprolite volume,  $m$  is saprolite mass, and  $\rho$  is saprolite density.  $\Delta V = V_f - V_i$ , the difference between the final and initial saprolite volumes. In a saprolite with porosity  $\phi$ , the fraction of the saprolite that is solid mass is  $(1 - \phi)$ . If we assume that all mineral grains within the saprolite are spheres with diameter  $D_s$ , then there are at least  $V_i/D_s^3$  mineral grains in the initial saprolite volume. We focus on dissolution of a single mineral type and if our chosen mineral constitutes a fraction of the saprolite,  $r$ , there are  $rV_i/D_s^3$  grains of our chosen mineral within the saprolite volume. Each spherical grain has a surface area,  $A_s$ , where

$$A_s = 4\pi(\frac{1}{2}D_s)^2. \quad (24)$$

The total surface area of our chosen mineral within the saprolite is  $A_s r V_i / D_s^3$ . With a mineral dissolution rate,  $R_D$  (generally in units of mol m<sup>-2</sup> s<sup>-1</sup>), and the molar mass of our chosen mineral,  $M$ , we can find the total decrease in saprolite mass due to chemical dissolution over the period of time that the mineral surfaces are exposed to water,

$$\frac{\Delta m}{\Delta t} = \frac{V_i M R_D A_s r (1 - \phi)}{D_s^3}. \quad (25)$$

Combining equations 23 and 25,

$$\frac{\Delta V}{\Delta t} = \frac{V_i M R_D A_s r (1 - \phi)}{D_s^3 \rho}, \quad (26)$$

where  $\rho$  is the density of our chosen mineral. We now turn this change in volume into a change in height by assuming that all mass loss results in vertical compaction. Thus,  $\Delta V = dx dy \Delta z$  and  $V_i = dx dy dz$ . Dividing through by  $dx dy$ , we find

$$E_c = \frac{\Delta z}{\Delta t} = \frac{dz M R_D A_s r (1 - \phi)}{D_s^3 \rho}, \quad (27)$$

where  $E_c$  is a chemical denudation rate, the rate of the downward movement of the soil-saprolite interface, and  $dz$  represents the thickness of the upper saprolite layer in which we account for mineral dissolution. We can simplify this equation further by recognizing that porosity in a saprolite or bedrock is small and so  $(1 - \phi) \approx 1$ . Thus our final equation is

$$E_c = \frac{dz M R_D A_s r}{D_s^3 \rho}. \quad (28)$$

### 4.3 Annual Storm Ensemble

Equation 28 defines a rate of denudation and this denudation occurs when the soil-saprolite interface is exposed to water. For a given rainstorm and hillslope form, we have an exposure time function that describes the exposure time *after* the water beneath the perched water table begins to drain. Of course, the soil-saprolite interface is also exposed to water during the rainstorm. Thus the total exposure time function is formed by summing the length of the rainstorm and the exposure time calculated for the drainage of the perched water table. In actuality, dissolution will continue to occur even after the perched water table flow drains below the soil-saprolite interface because water is still beneath the interface in the saprolite. However, to avoid delving deeper into the details of fluid movement in the saprolite and bedrock, we simply account for dissolution that occurs while the perched water table is above the soil-saprolite interface.

Multiplying the total exposure time by the denudation rate  $E_c$  (equation 28) results in a function of  $x$  that describes the downward movement of the soil-saprolite interface that occurs in response to a single storm. Because we are interested in the effects of chemical denudation over geomorphic timescales, we convert the denudation function to an annual denudation function by multiplying the denudation that occurs during one storm by the number of storms in a single year. This results in the general chemical denudation function,  $E_c(x)$ , which is in units of  $\text{m yr}^{-1}$ . This

function is directly applied in the hillslope evolution simulations to follow.

To find the annual chemical denudation function, we must estimate the number of storms in a single year. Because we later use the work of Ferrier et al. (2010) to estimate realistic chemical denudation rates and the field work for the study was performed in Rios Icacos, Puerto Rico, we use precipitation data from Rios Icacos in estimating net annual rainfall. El Yunque National forest, where the Rios Icacos watershed is located, can receive more than 300 cm of rain a year (USDA Forest Service). We use this annual rainfall amount to construct two alternate climates which we later use to explore the effects of climate on hillslope evolution. A "normal" climate has two three hour rainstorms every week with rainfall intensity of one cm per hour (annual precipitation of 312 cm, 104 storms per year). A "frequent rain" climate has eight three hour rainstorms of intensity 0.25 cm per hour (again, annual precipitation of 312 cm, 416 storms per year).

It is important to note that, due to the dynamics of the perched water table flow, there are scenarios in which the perched water table will not drain completely beneath the soil-saprolite interface before another storm occurs. In this case, certain portions of the soil-saprolite interface on a hillslope may be perennially "exposed". The three hour storm with intensity one cm per hour results in a perched water table that takes three days to drain completely beneath the soil-saprolite interface (Section 6.1, Figure 8) and thus we do not need to worry about overlapping water tables in our models (the same goes for the "frequent rain" climate, although we do not present perched water table results for the "frequent rain" climate). We use the "normal" climate in the majority of our simulations and we use the "frequent rain" climate only to examine the impact of differing climate on chemical denudation and hillslope evolution.

#### 4.4 Dissolution Rates and Chemical Denudation Rates

The annual storm ensembles and our chemical denudation function, equation 28, form the basis for our linkage of the hydrologic and geomorphic timescales. Connecting the two timescales requires averaging dissolution of minerals, which occurs on the timescales of days, as water passes through the saprolite, over timescales of years, over which hillslopes may evolve. Thus we must be careful to correctly interpret the geochemical processes that may occur at the soil-saprolite interface. Mineral dissolution rates,  $R_d$  in equation 28, are known to vary widely in the field and

laboratory. Thus we define all the parameters in equation 28 besides  $R_D$  and then explore how dissolution rates in the literature, along with our annual storm ensemble, effect our estimations of chemical denudation rates. We then compare our estimated chemical denudation rates to those found in the literature and we select values for  $R_D$  to use in our simulations. Our mineral of choice

**Table 4:** Parameters for the Chemical Denudation Function, Equation 28. Mineral specific values ( $M$ ,  $r$ , and  $\rho$ ) are chosen for Albite, which can often (along with similar minerals) make up more than 50% of a granite or other similar rocks.

Parameter	Value	Explanation
$dz$	0.1 m	Depth of saprolite in which we account for mineral dissolution.
$M$	$263.02 \text{ g mol}^{-1}$	Molar mass of chosen mineral, albite.
$A_s$	$4\pi(D_s/2)^2 = 3.14 \times 10^{-6} \text{ m}^2$	Estimated surface area of mineral grains.
$r$	0.5	Estimated proportion of saprolite made up of chosen mineral, albite.
$D_s$	0.001 m	Diameter of mineral grains.
$\rho$	$2.62 \times 10^6 \text{ g mol}^{-1}$	Density of chosen mineral, albite.

in modeling chemical dissolution is albite because albite dissolution has been studied widely and it forms a significant component of many rocks. We assume that albite makes up 50% of the saprolite ( $r = 0.5$ ). We arbitrarily select a mineral grain diameter of one mm. We set  $dz = 0.1$  m (Table 4) because that seems a reasonable estimate of the length scale of roughness at the soil-saprolite interface.

The idea that chemical denudation in the saprolite is related to the amount of time that the saprolite is exposed to water is predicated on the idea that water passing through the saprolite remains "fresh", that mineral dissolution rates do not decrease as water passes through. We can estimate the length of time that the saprolite thickness in which we account for mineral dissolution is exposed to water. The hydraulic conductivity of the saprolite material is on the order of  $10^{-7} \text{ m s}^{-1}$  or about  $3 \text{ m yr}^{-1}$  (Section 3.4). With our chosen values for  $dz$  and  $K$ , we know that it takes about 11 or 12 days for water to pass from the top to the bottom of our chosen saprolite thickness,  $dz$ . White and Brantley (2003) found that dissolution rates of plagioclase decrease parabolically over six years, but only decreases one order of magnitude during this time. Because the water causing dissolution in the upper 0.1 meters of saprolite is exposed to minerals for far less time than the time for which dissolution rates are known to decrease, it seems safe to assume that dissolution rates do not decrease significantly as water passes through the saprolite layer - the water

is always "fresh". Thus, for the remainder of this analysis, we assume that, using constant mineral dissolution rates, all saprolite minerals that can dissolve, during a given period of exposure time to water, will dissolve. We do not concern ourselves with the possibilities of saturated solutions or supply-limited dissolution. This assumption is consistent with the work of Maher (2010), who finds that chemical weathering rates are far more dependent on fluid flow than other factors such as mineral kinetics. It is worth noting that, contrary to what we assume occurs at shallow depths, at greater depths, groundwater is likely to become saturated with minerals and, as Jin et al. (2010) point out, chemical dissolution rates by groundwater may decrease downslope as the water becomes more saturated. We leave an analysis of deeper groundwater processes to another study.

Laboratory and field experiments reveal a range of mineral dissolution rates: White and Brantley (2003) report plagioclase dissolution rates around  $3.1 \times 10^{-13}$  mol m $^{-2}$  s $^{-1}$  at the onset of dissolution, Chen and Brantley (1996) report albite dissolution rates around  $10^{-11}$  to  $10^{-12}$  mol m $^{-2}$  s $^{-1}$  at room temperature for pH values varying from three to five. Westrich and Holden (1991) report dissolution rates as high as  $10^{-8}$  mol m $^{-2}$  s $^{-1}$  at low acid pHs and Welch and Ullman (1992) report dissolution rates from  $10^{-8}$  to  $10^{-12}$  mol m $^{-2}$  s $^{-1}$  for minerals in organic acid solutions. Field studies report relatively rapid dissolution rates, with Li (1976) reporting  $1.2 \times 10^{-10}$  mol m $^{-2}$  s $^{-1}$  and Ferrier et al. (2010) reporting  $4.17 \times 10^{-11}$  mol m $^{-2}$  s $^{-1}$ .<sup>1</sup>

We are inclined to use more rapid dissolution rates for a few reasons. First, laboratory and field measurements of mineral dissolution are known to vary many orders of magnitude and determining whether our definition hillslope has acidic rainfall solution, with carbonic acids and/or organic acids, is beyond the scope of this research<sup>2</sup>. Secondly, we believe that we are both underestimating the amount of saprolite exposed to dissolution (we only account for the upper 0.1 meters and saprolite can often be meters thick) and the amount of time the saprolite is exposed to water (we assume that exposure ends when the water table dips below the soil-saprolite interface when in reality, dissolution continues while water is below the interface but still within the

---

<sup>1</sup>Li (1976) reports dissolution rates in units of mg per mineral surface area per year and Ferrier et al. (2010) reports rates in units of mol per hectare of land area per year. Both rates were converted to units of mol m $^{-2}$  of mineral surface area per s $^{-1}$  by using the data in Table 4 and by assuming that all mineral dissolution is albite/plagioclase.

<sup>2</sup>On forested, soil-mantled hillslopes, rainfall may contain, in addition to carbonic acids derived from the atmosphere, organic acids dissolved as water passes through the soil column. If these acids are present in the subsurface fluids, then mineral dissolution rates could be quite high, as Welch and Ullman (1992) find.

saprolite). Thirdly, mineral dissolution rates on the order of  $10^{-9}$  and  $10^{-10}$ , when entered into equation 28 along with values from Table 4, give chemical denudation rates on the order of  $10^{-4}$  and  $10^{-5} \text{ m yr}^{-1}$ , the former of which is consistent with previous estimates by Roering et al. (2007) of denudation rates in the Oregon Coast Range and the latter of which is consistent with estimates by Velbel (1985) and Matmon et al. (2003) of denudation rates in the Appalachians.

## 4.5 Simulation Methodology

Using the analytically calculated drainage sequences of the perched water table after a given storm (Section 3.4) and our numerical algorithm, we estimate the net exposure time of the soil-saprolite interface to water. We then convert the exposure time from one storm to an annual exposure time and then to annual chemical denudation rate, as described in Sections 4.2, 4.3, and 4.4. These results are presented in Section 6.1.

## 5 Hillslope Evolution

The aim of this study is to examine how hillslope evolution is constrained by chemical and mechanical processes. We have already discussed our original formulation of chemical denudation on hillslopes. In this section we describe linear soil diffusion in our quasi two-dimensional framework and then we combine the chemical and mechanical processes in a hillslope mass balance equation. We then use the forward differencing method on the hillslope mass balance equation to numerically simulate hillslope evolution through time.

### 5.1 Soil Diffusion in the Quasi Two-Dimensional Framework

The linear diffusion model of mechanical erosion has been extensively explored in the literature (Culling, 1960; Dietrich, 2003; Mudd and Furbish, 2004; Anderson and Anderson, 2010). A general form of the linear soil diffusion equation in one dimension is

$$\frac{d\zeta}{dt} = \frac{dq_s}{dx} \quad (29)$$

in which

$$q_s = -D \frac{d\zeta}{dx} \quad (30)$$

where  $\zeta$  (as a reminder) is land surface elevation,  $q_s$  is soil flux, and  $D$  is a constant of diffusivity. Casting the linear diffusion equation into our quasi two-dimensional framework, we add the contour width function into the mass balance,

$$\frac{d}{dt}(b(x)\zeta) = \frac{d}{dx}(b(x)q_s). \quad (31)$$

Fernandes and Dietrich (1997) compile estimates of  $D$  from the literature, which range from  $4.4 \times 10^{-4} \text{ m}^2 \text{ yr}^{-1}$  (Nash, 1980b) to  $1 \times 10^{-3} \text{ m}^2 \text{ yr}^{-1}$  (Hanks et al., 1984) in semiarid climates, from  $5 \times 10^{-3}$  for coarse soils in Mediterranean climates (Reneau, 1988) to  $3.6 \times 10^{-2} \text{ m}^2 \text{ yr}^{-1}$  for clay-rich soils in humid to temperate environments (McKean et al., 1993). Because our earlier assumptions set our definition hillslope in a humid to temperate climate, we use a diffusivity value of  $10^{-2} \text{ m}^2 \text{ yr}^{-1}$  for the majority of our simulations, and a diffusivity value of  $10^{-3} \text{ m}^2 \text{ yr}^{-1}$  when examining

how changes to diffusivity can impact hillslope evolution.

## 5.2 Hillslope Mass Balance Equation

Because we are interested in the competing influences of mechanical and chemical weathering, the former contributing stability and smoothing out topographic variation and the latter potentially counteracting mechanical processes and introducing topographic variation, our hillslope model accounts only for mechanical diffusion of soil and for the downward movement of the soil-saprolite interface due to chemical erosion. Changes in topography are changes to the land surface,  $\zeta$ , which varies as a function of  $x$ , the distance from the top of the hillslope. Changes in the land surface are due to the downslope flux of soil, equation 31, and the denuding effects of chemical erosion,

$$\frac{d\zeta}{dt} = \frac{d}{dx}(q_s) + E_c(x). \quad (32)$$

As the soil-saprolite interface moves downward, so does the land surface because we assume that the soil thickness,  $H$ , is constant. Thus, we can place  $E_c(x)$  directly in the equation for changes in land surface. We cast the mass balance equation in our quasi two-dimensional framework, multiplying land surface, soil flux, and chemical erosion by the contour width function such that

$$\frac{d}{dt}(b(x)\zeta) = \frac{d}{dx}(b(x)q_s) + b(x)E_c(x). \quad (33)$$

Replacing the flux term,  $q_s$ , with the linear diffusion model (equation 30), pulling  $b(x)$  out of the time derivative term, and dividing through by  $b(x)$ , we retrieve our final analytical mass balance equation describing changes in land surface elevation with time,

$$\frac{d\zeta}{dt} = -\frac{D}{b(x)} \frac{d}{dx}\left(b(x) \frac{d\zeta}{dx}\right) + E_c(x). \quad (34)$$

It is important to note that for a given hillslope form, which is described by a unique planform and concavity, there is a specific contour width function,  $b(x)$ , and a specific chemical denudation function,  $E_c(x)$ . In running our hillslope simulations, we always make sure that  $b(x)$  and  $E_c(x)$  are consistent with the hillslope form of the initial condition.

### 5.3 Numerical Hillslope Model

We use the forward differencing method to model hillslope evolution through time. The forward difference approximation for land surface elevation takes the form

$$\zeta(t + \Delta t) = \zeta(t) + \Delta t \frac{d\zeta}{dt}. \quad (35)$$

We now replace the time derivative term with equation 34,

$$\zeta(t + \Delta t) = \zeta(t) - \frac{\Delta t D}{b(x)} \frac{d}{dx} \left( b(x) \frac{d\zeta}{dx} \right) + \Delta t E_c(x). \quad (36)$$

All continuous functions of  $x$  and/or  $t$  must be converted to discrete functions for the numerical method to work. We use the symbols  $i$  and  $j$  in discretizing our equation, where  $i$  takes the place of  $x$  and  $j$  the place of  $t$ . Thus,  $\zeta(t + \Delta t)$ , which represents the hillslope land surface at time  $(t + \Delta t)$  over the entire  $x$  domain  $[0, L]$  becomes  $\zeta_{i,j+\Delta t}$ ,  $E_c(x)$  becomes  $E_{ci}$ , and  $b(x)$  becomes  $b_i$ .

Discretizing the diffusive term,

$$\frac{d}{dx} \left( b(x) \frac{d\zeta}{dx} \right), \quad (37)$$

takes multiple steps. First, we set

$$A = b(x) \frac{d\zeta}{dx} \quad (38)$$

such that

$$\frac{d}{dx} \left( b(x) \frac{d\zeta}{dx} \right) = \frac{A_{i+\frac{1}{2}} - A_{i-\frac{1}{2}}}{\Delta x}. \quad (39)$$

Recognizing that

$$A_{i+\frac{1}{2}} = b_{i+\frac{1}{2}} \left. \frac{d\zeta}{dx} \right|_{x=1+\frac{1}{2}} = \frac{b_{i+1} + b_i}{2} \frac{\zeta_{i+1} - \zeta_i}{\Delta x} \quad (40)$$

and

$$A_{i-\frac{1}{2}} = b_{i-\frac{1}{2}} \left. \frac{d\zeta}{dx} \right|_{x=1-\frac{1}{2}} = \frac{b_i + b_{i-1}}{2} \frac{\zeta_i - \zeta_{i-1}}{\Delta x}. \quad (41)$$

Thus,

$$\zeta_{i,j+\Delta t} = \zeta_{i,j} - \frac{\Delta t D}{\Delta x b_i} \left( \frac{b_{i+1} + b_i}{2} \frac{\zeta_{i+1} - \zeta_i}{\Delta x} - \frac{b_i + b_{i-1}}{2} \frac{\zeta_i - \zeta_{i-1}}{\Delta x} \right) + \Delta t E_{ci}. \quad (42)$$

Equation 42 is the discrete, forward difference numerical approximation of  $\zeta(x, t)$ , which can be used to simulate hillslope evolution through time, given an initial condition  $\zeta_{i,j}$ , a discrete contour width function function  $b_i$ , a discrete chemical erosion function  $E_{ci}$ , a time step  $\Delta t$ , a space step  $\Delta x$ , and a constant  $D$ .

## 5.4 Initial Conditions

For all of our simulations, we use the hillslope forms described in Section 2.4 as initial conditions.

## 5.5 Boundary Conditions

The finite differencing method described above requires boundary conditions at both ends of the  $x$  domain and different simulations require different boundary conditions. For simulations involving both soil diffusion and chemical erosion, the boundary conditions are the denudation rates determined by the chemical denudation function  $E_c$  (i.e.  $E_c(0)$  and  $E_c(L)$ ). For simulations involving only soil diffusion (where  $E_c = 0$ ), the boundary conditions differ from one end of the  $x$  domain to the other: at  $x = 0$ , a Neumann condition is imposed such that  $\frac{d\zeta}{dx} = 0$  (a no-flux boundary), and at  $x = L$ , the boundary condition is determined by the chemical denudation rate of the uniform hillslope. We use chemical denudation rates in the diffusion-only simulations so that we can directly compare the simulations involving chemical processes to those that do not. We might think of the denudation rate at  $x = L$  in the diffusion-only simulations as downcutting caused by a stream channel at the bottom of the hillslope. It is worth mentioning that the Neumann condition forces the planar and concave hillslopes into unexpected shapes, with the hillslope crests achieving a slope of zero over short periods of hillslope evolution. Because the Neumann condition is physically correct, as it places a no-flux boundary for soil diffusion at  $x = 0$ , and because the Neumann boundary condition does not cause changes far downslope over the geomorphic timescales that we examine hillslope evolution, we accept its effects. We apply the chemical denudation rate from a uniform hillslope to convergent, uniform, and divergent hillslopes so that all three hillslopes are downcut at  $x = L$  at the same rate, such that no differences are created by chemical denudation rates in the diffusion-only simulations.

## 5.6 Hillslope Simulation Parameters

We run various simulations using equation 42, some accounting for both soil diffusion and chemical erosion and some accounting for only soil diffusion. We change many parameters in exploring hillslope evolution, but a few are kept constant throughout. These are listed in Table 5.

**Table 5:** Hillslope Evolution Simulation Parameters

Parameter	Value	Explanation
$\Delta t$	10 years	Simulation Time Step
$\Delta x$	one meter	Simulation Space Step
$L$	100 meters	Hillslope Length

## 5.7 Calculating Denudation Ratios

It is informative to compare the mass denuded by mechanical and chemical processes during a given time period of hillslope evolution. Mudd and Furbish (2004) propose an equation of the form

$$\theta_d = \frac{R_c}{R_c + R_m} \quad (43)$$

where  $\theta_d$  is called the denudation ratio,  $R_c$  is the total chemical denudation over a given period of time, and  $R_m$  is the total mechanical denudation over the same period of time. We can calculate both  $R_c$  and  $R_m$  during our hillslope simulations and thus can examine the denudation ratios in each of our simulations.  $R_c$  is calculated rather simply. The  $E_c$  function (Section 4.2) describes net chemical denudation in a single year as a function of  $x$ . We can simply integrate the function  $E_c(x)$  over its domain and multiply the result by contour width to find the total volume of material lost to chemical erosion.  $R_m$  can be calculated rather simply as well. The material transported away from the hillslope by soil diffusion is the amount of soil that passes out of the hillslope at  $x = L$ . The linear diffusion equation (Section 5.1) states that the flux of soil is proportional to the slope of the hillslope by the diffusivity constant. Thus we can simply calculate the flux of soil at  $x = L$  at each time step in our hillslope simulations and sum the total volume of soil that is fluxed out of the hillslope over the total time that the hillslope is allowed to evolve. Because the densities of soil and saprolite are approximately equal (Ferrier et al., 2010), we need not convert volume to mass to find the denudation ratio. For each hillslope evolution simulation, we calculate  $\theta_d$  to quantify

and compare the influence of mechanical and chemical processes.

## 5.8 Simulation Methodology

We run a variety of hillslope evolution simulations to explore how hillslopes are sensitive to a variety of parameters. Each simulation focuses on the effect of changing one parameter. We run and present each simulation in a similar manner. A single simulation produces a plot that shows the evolution of three hillslopes, the convergent, uniform, and divergent planforms of one chosen concavity (convex, planar, or concave). For example, a single simulation on a convex hillslope in which convergence rate is varied shows six evolved hillslopes that share a single initial hillslope profile condition: two convergent convex hillslopes with different convergence rates, two uniform convex hillslopes with different convergence rates, and two divergent convex hillslopes with different divergence rates. This methodology allows us to focus on the differences in the evolution of hillslopes that differ by their planform. If convergent hillslopes erode lower than divergent hillslopes, which would increase the magnitude of the hillslope convergence/divergence factor on the convergent/divergent hillslopes, a positive feedback mechanism may contribute to hillslope evolution. Comparing the differences between two sets of convergent and divergent hillslopes that differ by some parameter allows us to observe how different parameters exaggerate or attenuate the differences in evolution between hillslopes of different planform and how different parameters exaggerate or attenuate the influence of a chemical erosion positive feedback mechanism.

We run 5 sets of hillslope evolution simulations. The first set (Section 6.2.1) involves only mechanical-diffusive processes and we use these simulations as a reference point to understand the impacts of chemical denudation in other simulations. The second set (Section 6.2.2) varies the strength of chemical denudation to explore whether, and at what chemical denudation rates, chemical processes impact hillslope evolution. The third set (Section 6.2.3) allows us to examine whether differences in planform (convergence and divergence rates), which influence the intensity of chemical erosion, are large enough to influence hillslope evolution. We expect that larger convergence rates (a more negative  $c$  value) will result in more intense denudation and larger divergence rates (a more positive  $c$  value) in less intense denudation, which would suggest that a chemical denudation positive feedback mechanism is an important factor in hillslope evolution. The fourth set (Section 6.2.4) examines how rainstorm intensity and frequency influence chemical

denudation and hillslope evolution. The fifth and final set (Section 6.2.5) explores under what conditions relatively low chemical denudation rates may still play a role in hillslope evolution. For each of the 5 sets, we run simulations on convex, planar, and concave hillslopes, but do not present all the results in the following section. Any simulations not presented in Section 6.2 are presented in Section 9.

## 6 Results and Discussion

### 6.1 Perched Water Table Flow and Chemical Denudation

Our first simulation estimates the drainage of a water table perched above the soil-saprolite interface after the end of a single rainstorm. Drainage sequences are shown for all nine hillslopes in Figure 7, which demonstrates how the dynamics of the perched water table differ significantly from hillslope to hillslope. The concave hillslopes (subplots 1, 2, and 3) maintain a perched water table for the longest period of time. Because the speed of water beneath the perched water table is proportional to the slope over which it flows (this is the basis of the kinematic wave approximation) and because the slope of the concave hillslope decreases downslope, the speed of the water decreases downslope, and water gathers towards the bottom of the slope. The planar hillslopes (subplots 4, 5, and 6) clearly demonstrate the dynamics of the kinematic wave approximation. Because the slope is constant on the planar hillslopes, the water table propagates downslope at a constant velocity, and because saprolite conductivity is constant, the water table drains downward uniformly and at a constant rate. On the uniform planar hillslope (subplot 5), the kinematic wave speed of the perched water table is constant and the initial water table form is translated vertically downwards and horizontally downslope. On the convergent planar (subplot 4) and divergent planar (subplot 6) hillslopes, this same basic behavior is demonstrated although altered slightly due to the convergent and divergent natures of the hillslopes. The convex hillslopes (subplots 7, 8, 9) drain the fastest due to the increase in slope (and kinematic wave speed) downslope. The convex hillslopes demonstrate the clearest difference between convergent and divergent hillslopes. After 18 hours of drainage, the perched water table still covers most of the convergent convex hillslope while the perched water table only covers a small section of the divergent convex hillslope. All of the drainage simulations demonstrate that the perched water table is largest and seems to last longest on the convergent hillslopes.

For a given rainstorm and the resultant drainage sequences (Figure 7) we can use the process described in Section 4.1 to find the amount of time the soil-saprolite interface is exposed to water as it varies with distance from the hillslope crest. The exposure times corresponding to the drainage sequences shown in Figure 7 are shown in Figure 8. The concave hillslopes (subplots 1,2,3) have the largest exposure times towards the bottom due to the decreasing slope and resultant gathering

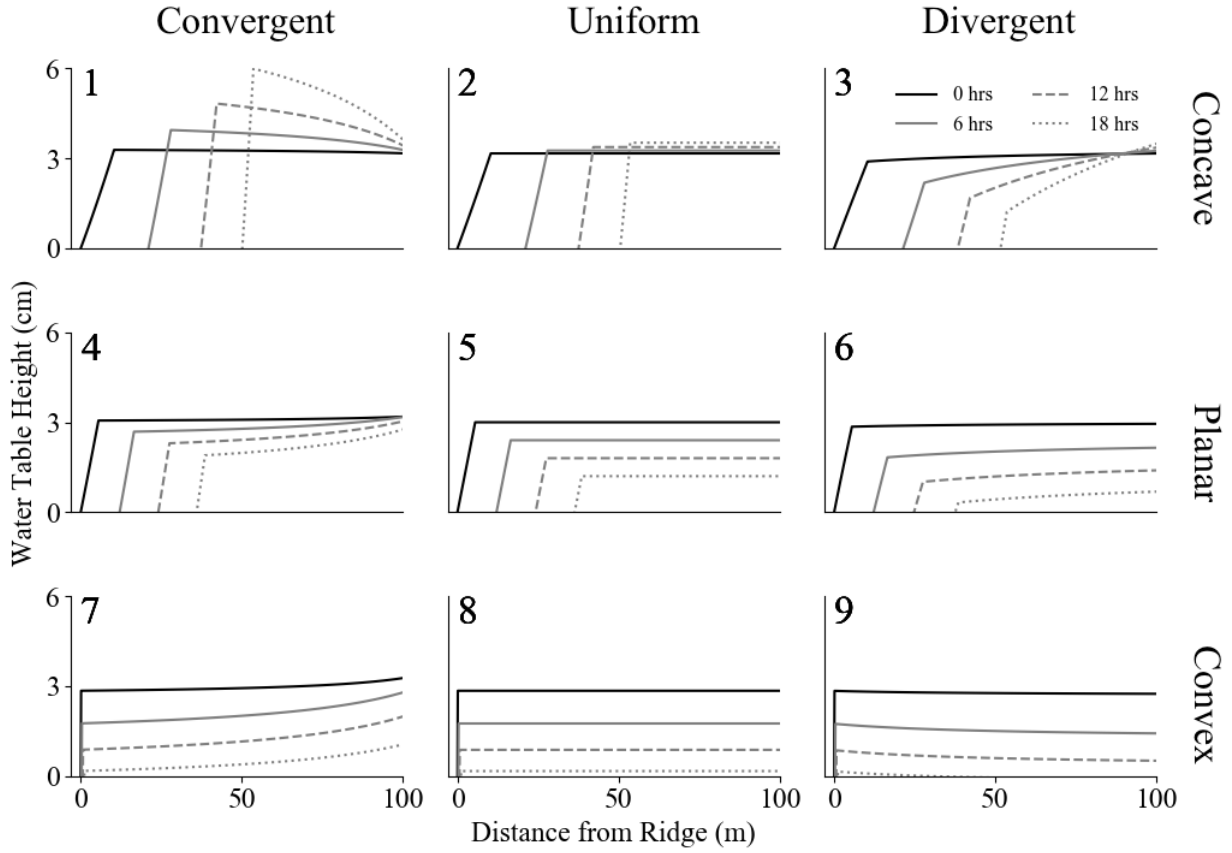


**Figure 7:** The water table height above the soil-saprolite interface along the length of the hillslope on nine hillslopes. The water table height is shown after 0 (black line), 6 (gray line), 12 (dashed line), and 18 (dotted line) hours of drainage and can be seen flowing downslope and infiltrating into the underlying saprolite. The water table is formed from a three hour rainstorm with precipitation intensity of one  $\text{cm hr}^{-1}$ . Plots correspond to the unique hillslope forms in figure 5; concavity and planform are labeled by column and row.

of water towards the bottom of the hill. The concave hillslopes have minimal exposure towards the top of the hill where slope is steepest and water drains away very quickly. The difference in exposure times is apparently small between the concave hillslopes of different planform. The planar hillslope demonstrates significant variation in exposure time between the hillslopes of different planform, with the convergent planar hillslope (subplot 4) experiencing more exposure than the uniform planar (subplot 5), which experiences more exposure than the divergent planar hill-slope (subplot 6). All of the planar hillslopes have increasing exposure time towards the bottom of the hill. The convex hillslopes also demonstrate varied behavior. Exposure on the convergent convex hillslope (subplot 7) increases nonlinearly downslope and exposure on the divergent convex hillslope (subplot 9) decreases nonlinearly downslope. The uniform convex hillslope (subplot

8) experiences mostly uniform exposure, apparently because the increasing slope and fluid flow speed downslope counteract the effects of water gathering downslope.

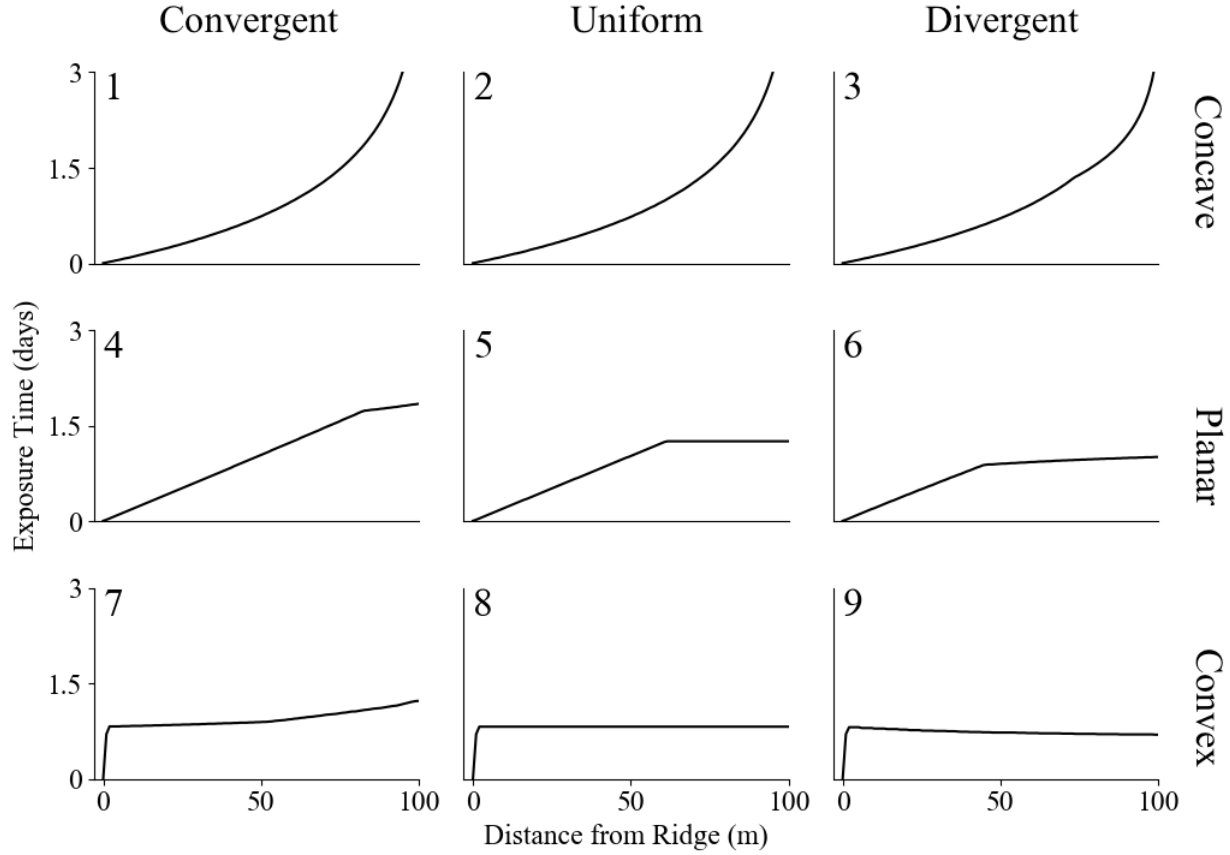


**Figure 8:** Exposure time after one storm as it varies with distance from the hillslope ridge. Exposure time is calculated for a single three hour storm with an intensity of one  $\text{cm hr}^{-1}$ .

We calculate annual chemical denudation rates using the exposure times shown in Figure 8 and the process described in Section 4. The chemical denudation rates are directly proportional to exposure time and demonstrate the same dynamics. We can now see how perched water table dynamics influence the amount of chemical denudation occurring on various hillslopes. Concave hillslopes (subplots 1,2, and 3) experience far greater chemical denudation at the bottom of their slopes than at the top. Planar hillslopes (subplots 4,5, and 6) also experience increasing denudation downslope. It is interesting to note that of the convex hillslopes, the convergent convex hillslope (subplot 7) experiences the greatest amount of chemical denudation towards the bottom of the slope, like most of the other hillslopes, while the divergent convex hillslope (subplot 9) experiences the greatest amount of chemical denudation towards the top of the slope. This is a result of the fact that fluid beneath the perched water table, in addition to flowing downslope, flows vertically

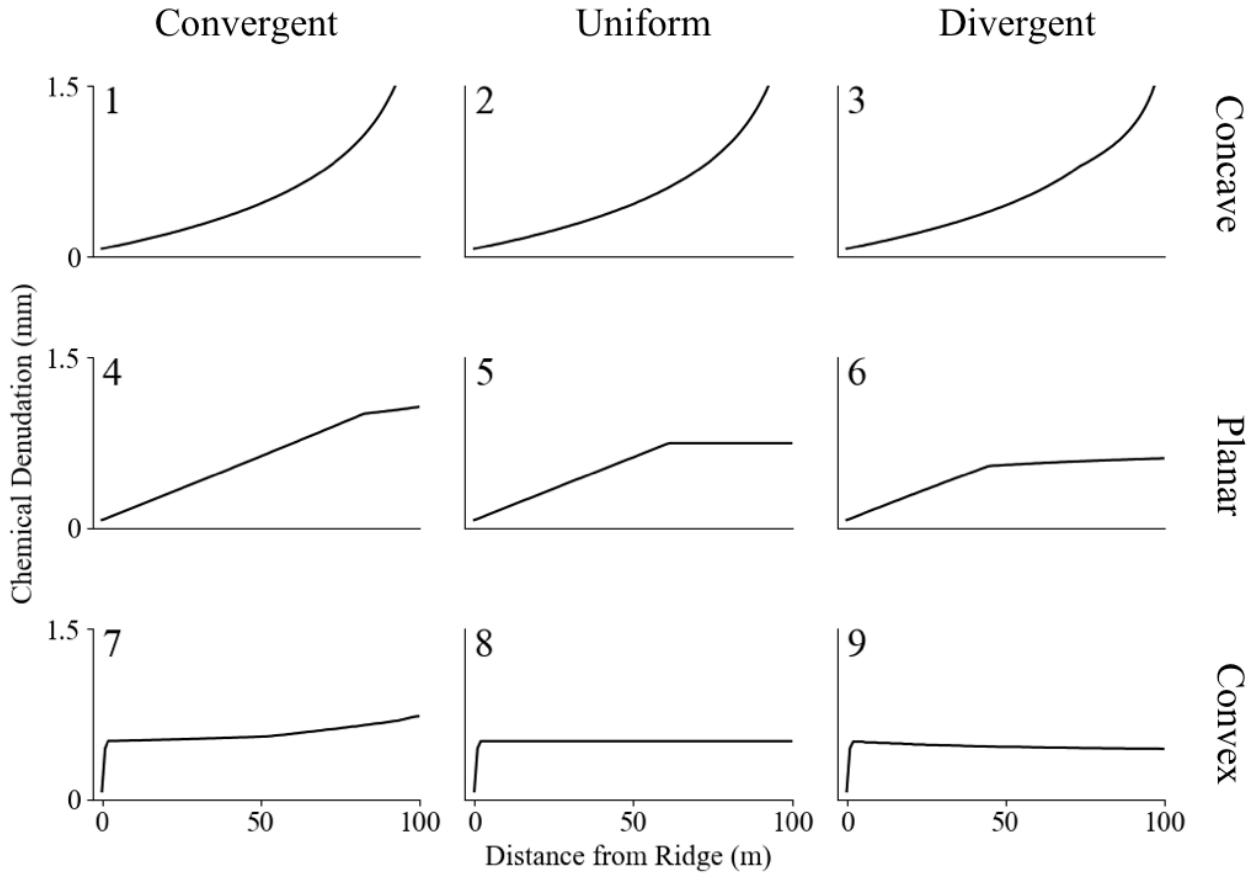


**Figure 9:** Annual chemical denudation assuming that one three hour storm with a precipitation intensity of one  $\text{cm hr}^{-1}$  occurs twice a week for an entire year.

downward into the saprolite. Varying the infiltration rate into the saprolite might attenuate or exaggerate the "humped" geometry of subplot 9.

Our model demonstrates how hillslope geometry influences perched water table flow and how that flow influences the emergent behavior of chemical denudation. Convergent hillslopes (subplots 1, 4, 7) experience a greater amount of chemical erosion than other planforms due to convergent subsurface hydrologic flow. Divergent hillslopes experience a lesser amount of chemical erosion and uniform hillslopes experience somewhere in between.

We now wish to integrate our estimated chemical erosion rates into hillslope evolution simulations. The kinematic wave approximation for perched water table flow has its limitations, particularly the required boundary condition that the water table height is always zero at the hillslope crest,  $h = 0$  at  $x = 0$ . These limitations extend into the estimations of exposure time and chemical denudation rates. For the purposes of simplicity and parsimony, we now simplify the chemical

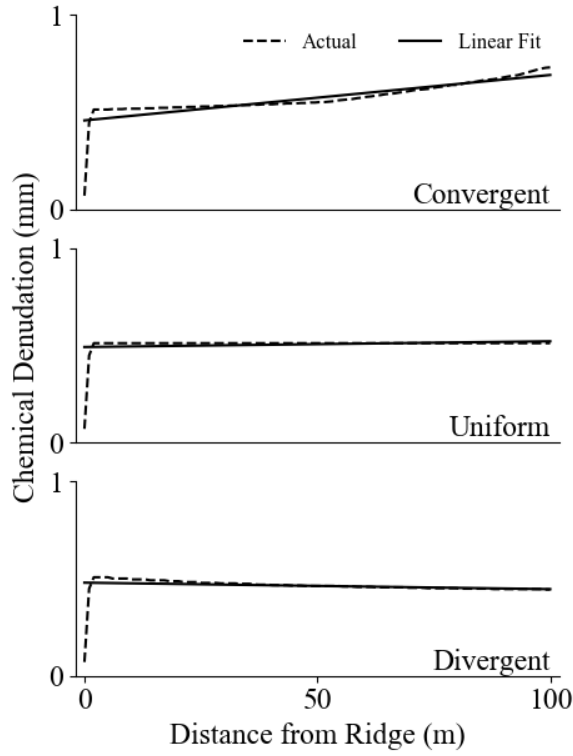


**Figure 10:** Annual chemical denudation on three convex parabolic hillslopes. From top to bottom, convergent, uniform, and divergent.

erosion functions while retaining the important behavioral differences among the hillslope forms. We perform linear regressions on each of chemical denudation functions presented in Figure 9 and use the lines of best fit for the  $E_c$  function in equation 42 (Section 4.3). Convex hillslope chemical denudation functions and their respective lines of best fit are shown in Figure 10.

## 6.2 Hillslope Evolution Simulations

### 6.2.1 Diffusion Only Simulations

Figure 11 shows a convex hillslope evolving over 30,000 years with only mechanical erosion (soil diffusion) operating. This simulation demonstrates the principle of diffusion-induced stability. All of the hillslopes evolve similarly, indicating that little to no topographic variation would be observed among the hillslopes of different planshapes. Any differences between the three hillslopes are likely a product of our selected boundary conditions and even if they are not, no mechanism

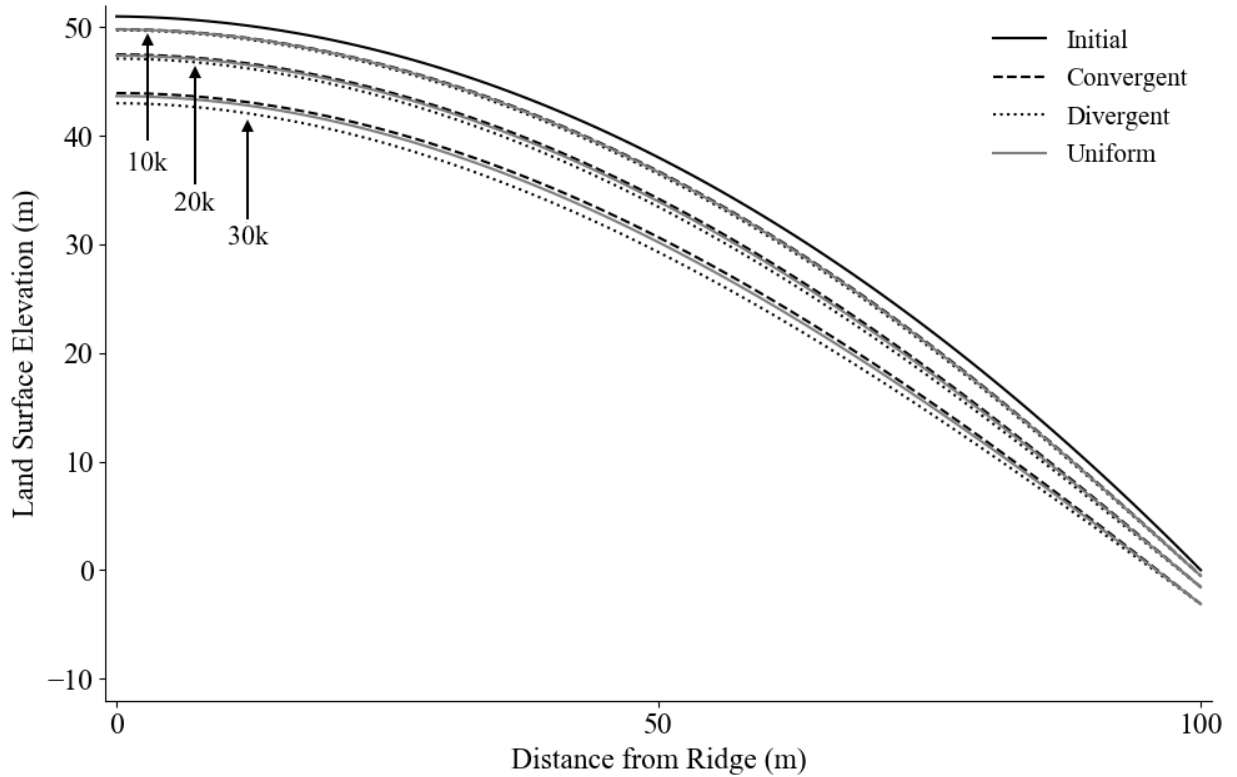


**Figure 11:** Hillslope evolution after 10,000, 30,000, and 60,000 years with mechanical soil diffusion only. Convex hillslope,  $D = 0.01 \text{ m}^2 \text{ yr}^{-1}$ .

would compound the preferential lowering of divergent hillslopes. These results are consistent with the stable behavior of linear soil diffusion observed by Mudd and Furbish (2004) and mathematically confirmed by Furbish and Fagherazzi (2001). This simulation is also consistent with findings that hillslopes undergoing linear soil diffusion and steady uplift have a parabolic steady state form. Even though our simulations explore the transient case, a general parabolic shape is maintained. See Section 9 for diffusion only simulations on planar and concave hillslopes.

### 6.2.2 Varying the Strength of Chemical Erosion

Figure 12 shows the evolution of a convex hillslope over 10,000 years undergoing both mechanical and chemical erosion. Two simulations are shown, the first with a chemical erosion rate of  $5 \times 10^{-4} \text{ m yr}^{-1}$  (strong  $E_c$ ) and the second with a chemical erosion rate of  $5 \times 10^{-5} \text{ m yr}^{-1}$  (weak  $E_c$ ). The simulation makes it evident that with weaker chemical erosion rates, the evolution of the hillslopes of different planforms do not differ by much at all. It appears that soil diffusion is strong enough

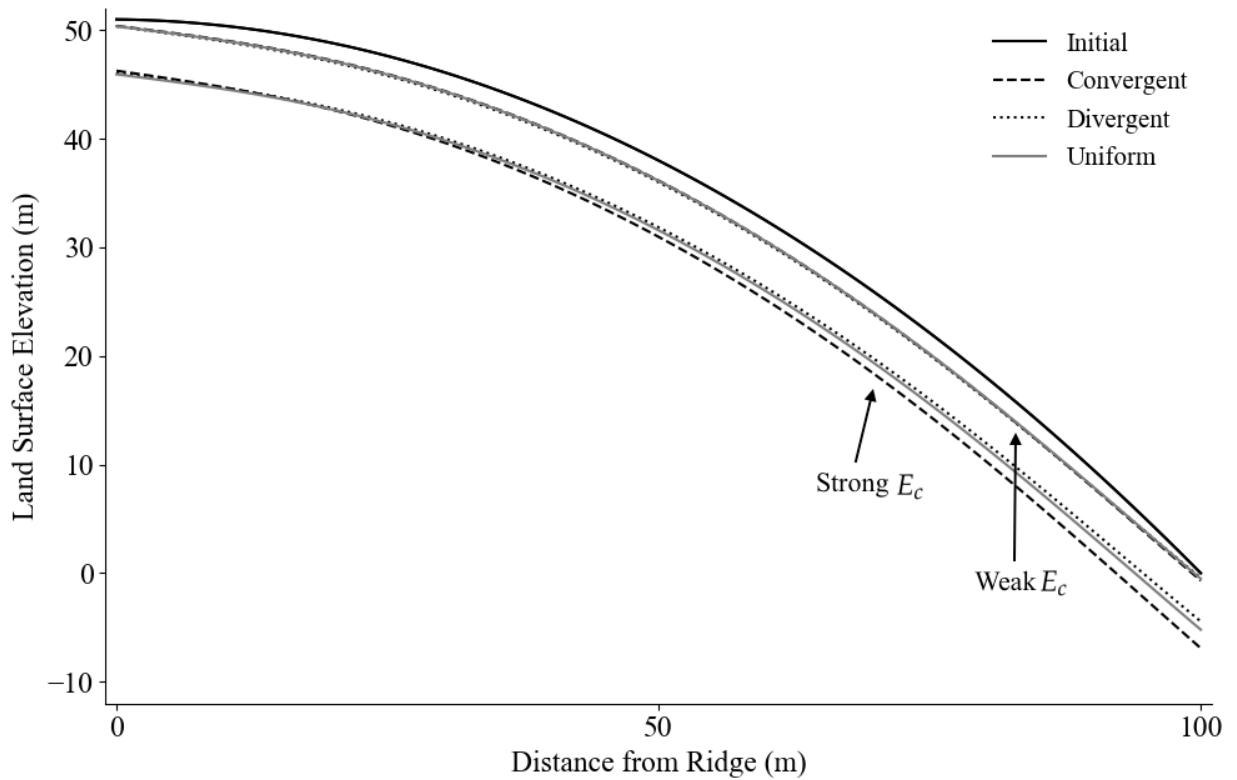


**Figure 12:** Hillslope evolution with soil diffusion and chemical erosion. Varying strength of chemical erosion with  $R_{dis} = 2 \times 10^{-9}$  and  $2 \times 10^{-10} \text{ mol m}^2 \text{ s}^{-1}$ . Convex hillslope, 10,000 year simulation,  $D = 0.01 \text{ m}^2 \text{ yr}^{-1}$ ,  $c = 0.2$ ,  $N = 0.009 \text{ m hr}^{-1}$ , 104 storms per year. Resultant chemical denudation rates when averaged over the planforms are approximately  $5 \times 10^{-4}$  and  $5 \times 10^{-5} \text{ m yr}^{-1}$ , respectively, with denudation ratios averaged over the planforms approximately 0.90 and 0.47.

to keep pace with and smooth out any topographic variation introduced by chemical erosion or the differences among the hillslopes are too small to observe. The convex hillslope simulation with weak chemical erosion rates has a denudation ratio of 0.47, demonstrating that diffusive mass flux approximately equals chemical mass flux.

At stronger chemical denudation rates the evolutions of the three hillslopes with different planforms proceed differently. The convergent hillslope is eroded deeper than the uniform hillside, and the uniform hillslope is eroded deeper than the divergent hillslope. This behavior is consistent with the results of Figure 9, which demonstrate that the convergent hillslope experiences the greatest amount of chemical erosion, particularly towards the bottom of the hillslope. The convergent hillslope is eroded less at the very top of the hill than the divergent hillslope, but the difference is small compared to the differences observed throughout the rest of the  $x$  domain.

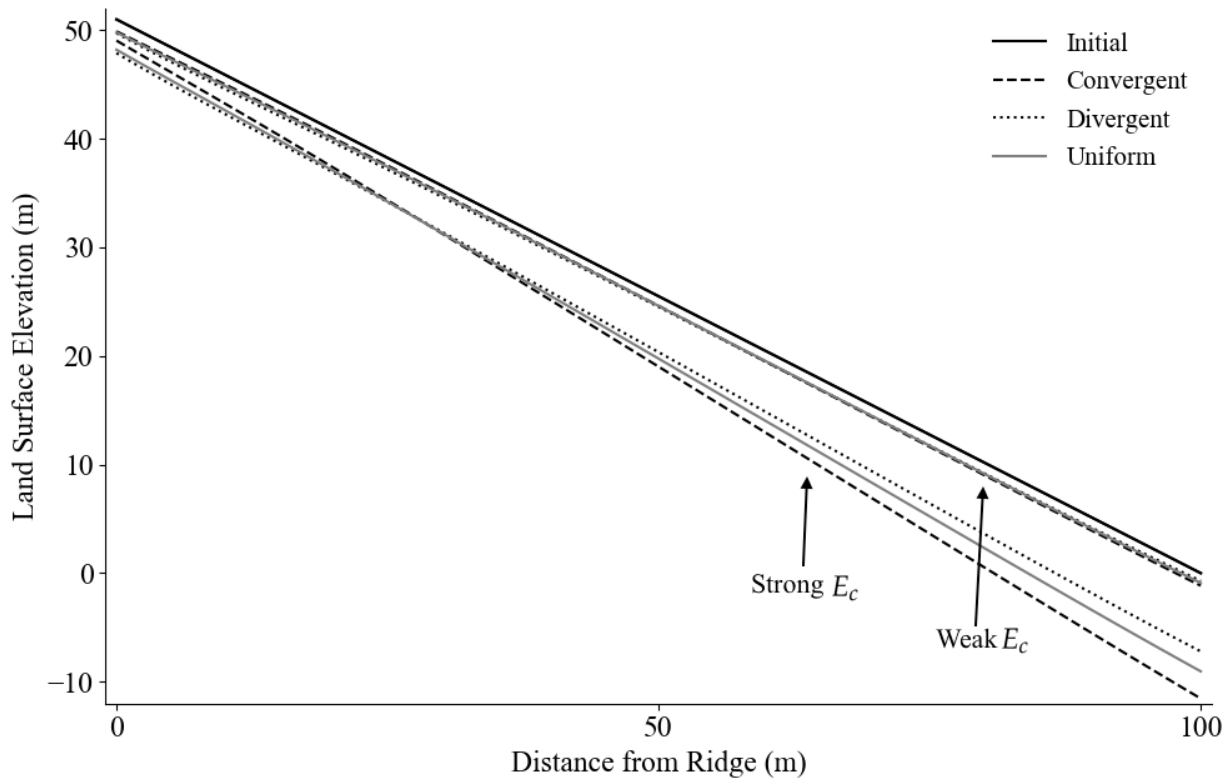


**Figure 13:** Hillslope evolution with soil diffusion and chemical erosion. Varying strength of chemical erosion with  $R_{dis} = 2 \times 10^{-9}$  and  $2 \times 10^{-10} \text{ mol m}^2 \text{ s}^{-1}$ . Planar hillslope, 10,000 year simulation,  $D = 0.01 \text{ m}^2 \text{ yr}^{-1}$ ,  $c = 0.2$ ,  $N = 0.009 \text{ m hr}^{-1}$ , 104 storms per year. Resultant chemical denudation rates when averaged over the planforms are approximately  $5 \times 10^{-4}$  and  $5 \times 10^{-5} \text{ m yr}^{-1}$ , respectively, with denudation ratios averaged over the planforms approximately 0.94 and 0.64.

With strong chemical erosion, the denudation ratio is approximately 0.90, indicating that chemical erosion dominates over diffusion.

Figure 13 shows an identical simulation run on an initially planar hillslope. This simulation shows the same basic results as the simulation on the convex hillslope, but, in the planar hillslope simulation, the convergent and divergent hillslopes differ by a greater degree. This indicates that on planar hillslopes chemical erosion may have a more significant erosive effect and we might expect planar hillslopes to develop more varied topography due to convergent hydrologic flow than convex hillslopes.

This is consistent with the physics of perched water table flow, which dictates that water lasts longer towards the bottom of the planar hillslope than the convex hillslope because the slope is steeper towards the bottom of the convex hillslope. This results in a greater annual denudation

rate on the planar hillslopes (Figure 9). With the stronger chemical erosion rates the denudation ratio on the planar hillslope is approximately 0.94 and chemical erosion dominates. With the weaker chemical erosion rates, the denudation ratio is 0.64.

Mudd and Furbish (2004) compile denudation ratios reported in the literature for a variety of river basins and show that ratios vary from 0.50 to 0.94. This lends some credibility to the simulations that produce high denudation ratios and demonstrate varied topography between hillslopes with convergent and divergent planforms. Velbel (1985) found that the advance of the weathering front into rock may proceed on the order of  $10^{-5}$  m yr $^{-1}$  and proposed an average Appalachian denudation rate of  $4 \times 10^{-5}$  m yr $^{-1}$ . Roering et al. (2007) found that total denudation rates in the Oregon coast range may be on the order of  $10^{-4}$  m yr $^{-1}$ . These estimates, along with the simulations presented thus far, indicate that perhaps in some locales chemical erosion is strong enough to overcome the smoothing effects of soil diffusion and cause a positive feedback, whereby lowered convergent sections of hillslope become further eroded.

If chemical erosion is sufficiently strong, the positive feedback mechanism may play out as we predicted, with convergent hillslopes experiencing preferential chemical erosion and likely becoming more convergent as a result. Perhaps the adjustment of other parameters influences the strength of the positive feedback effect and we explore such possibilities in further simulations. Because we see the positive feedback mechanism playing out with a chemical denudation rate on the order of  $10^{-4}$  m yr $^{-1}$ , we use the same mineral dissolution rate,  $R_D$ , that we used to calculate this higher chemical erosion rate,  $2 \times 10^{-9}$  mol m $^2$  s $^{-1}$ , in most of the following simulations. Using the higher estimates of chemical denudation allows us to explore the dynamics of hillslope evolution in response to chemical erosion that is sufficiently strong to introduce topographic variety.

### 6.2.3 Varying Convergence Rate

Figure 14 shows the evolution of a convex hillslope over 10,000 years. Two simulations are shown, the first with a convergence rate of  $c = \pm 0.2$  and the second with a convergence rate of  $c = \pm 0.35$  (negative for the convergent and positive for the divergent hillslope). The evolution of the uniform hillslope (which has a convergence rate of 0) does not differ between the two simulations and the evolution of the divergent hillslope differs only slightly (thus the two eroded divergent hillslopes overlap). The evolution of the two convergent hillslopes produces observable differ-

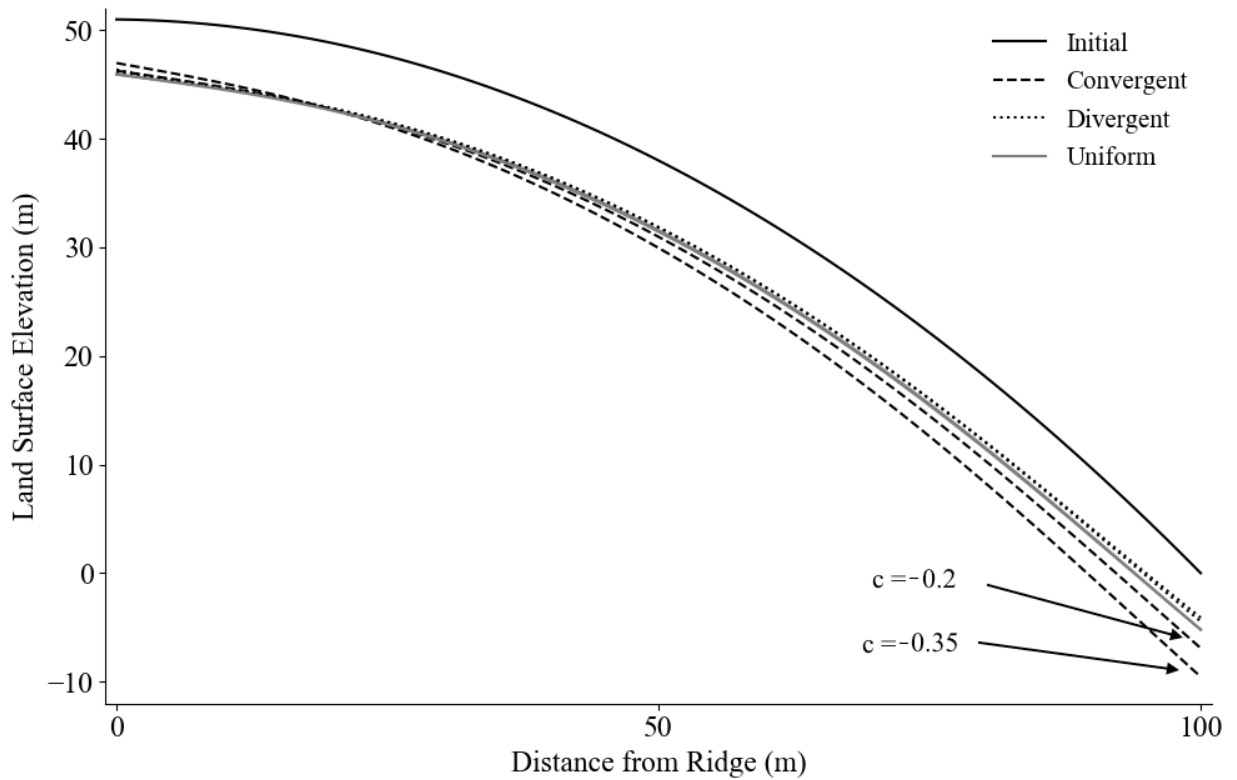


**Figure 14:** Hillslope evolution with soil diffusion and chemical erosion. Varying convergence rate from 0.2 to 0.35. Convex hillslope, 10,000 year simulation,  $D = 0.01 \text{ m}^2 \text{ yr}^{-1}$ ,  $R_{dis} = 2 \times 10^{-9} \text{ mol m}^2 \text{ s}^{-1}$ ,  $N = 0.009 \text{ m hr}^{-1}$ , 104 storms per year. Resultant chemical denudation rates for simulations with both convergence rates, when averaged over the planforms, are approximately  $5 \times 10^{-4} \text{ m yr}^{-1}$  with denudation ratios for simulations with both convergence rates, when averaged over the planforms, are approximately 0.90. Note that the two uniform hillslopes perfectly overlap because  $c = 0$  for both and the two divergent hillslopes are essentially overlapping due to minimal differences in net chemical and mechanical erosion.

ences. A greater convergence rate causes the convergent hillslope to erode a few extra meters. This simulation lends further credibility to a chemical erosion positive feedback mechanism occurring during hillslope evolution and suggests that chemical erosion leads hillslopes to evolve diverse and swale-like topographies.

If a section of hillslope is convergent, it experiences preferential chemical erosion. This erosion causes deepening, which causes the convergence rate of that section of hillslope to increase. We see in Figure 14 that a hillslope section with a higher convergence rate will preferentially erode, which will create a greater convergence rate, which will cause further preferential erosion, and so on. It is interesting that the divergent hillslope with the convergence rate of greater magnitude (0.35) does not erode significantly less than the divergent hillslope with the convergence rate of lesser

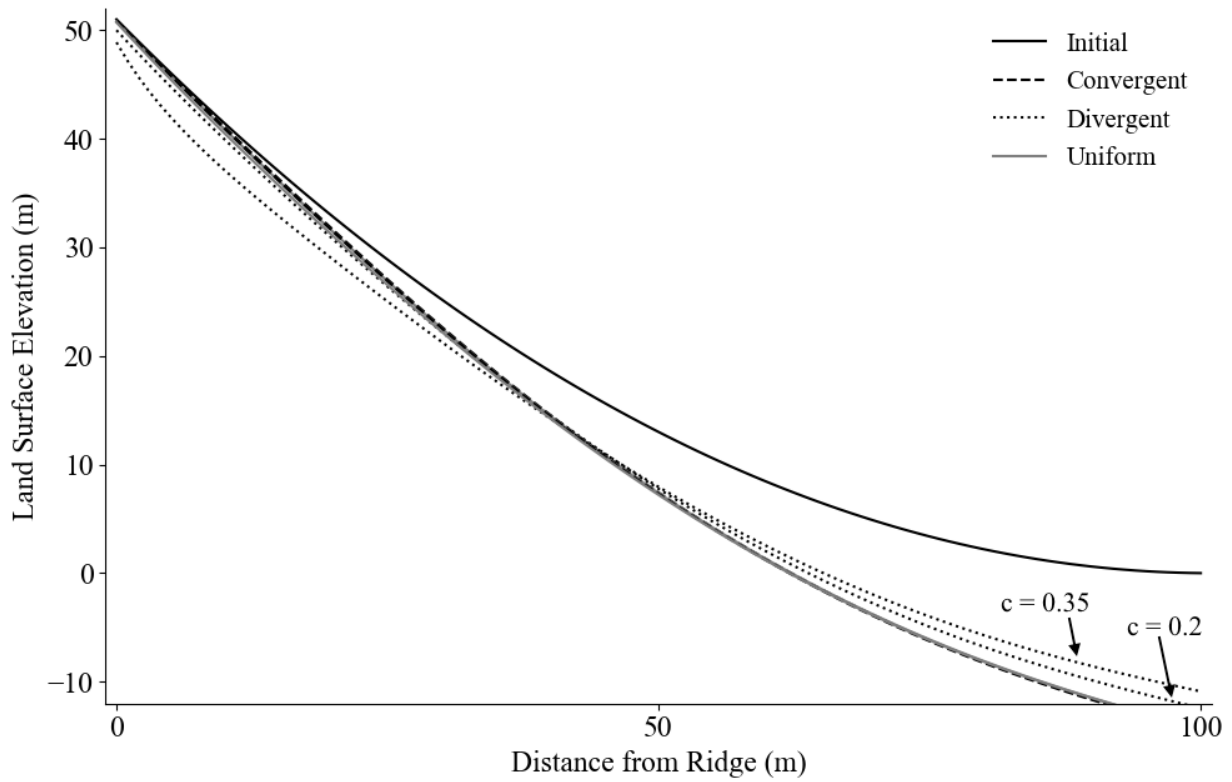


**Figure 15:** Hillslope evolution with soil diffusion and chemical erosion. Varying convergence rate from 0.2 to 0.35. Concave hillslope, 10,000 year simulation,  $D = 0.01 \text{ m}^2 \text{ yr}^{-1}$ ,  $R_{dis} = 2 \times 10^{-9} \text{ mol m}^2 \text{ s}^{-1}$ ,  $N = 0.009 \text{ m hr}^{-1}$ , 104 storms per year. Resultant chemical denudation rates for simulations with both convergence rates, when averaged over the planforms, are approximately  $6 \times 10^{-4} \text{ m yr}^{-1}$  with denudation ratios for simulations with both convergence rates, when averaged over the planforms, are approximately 0.99.

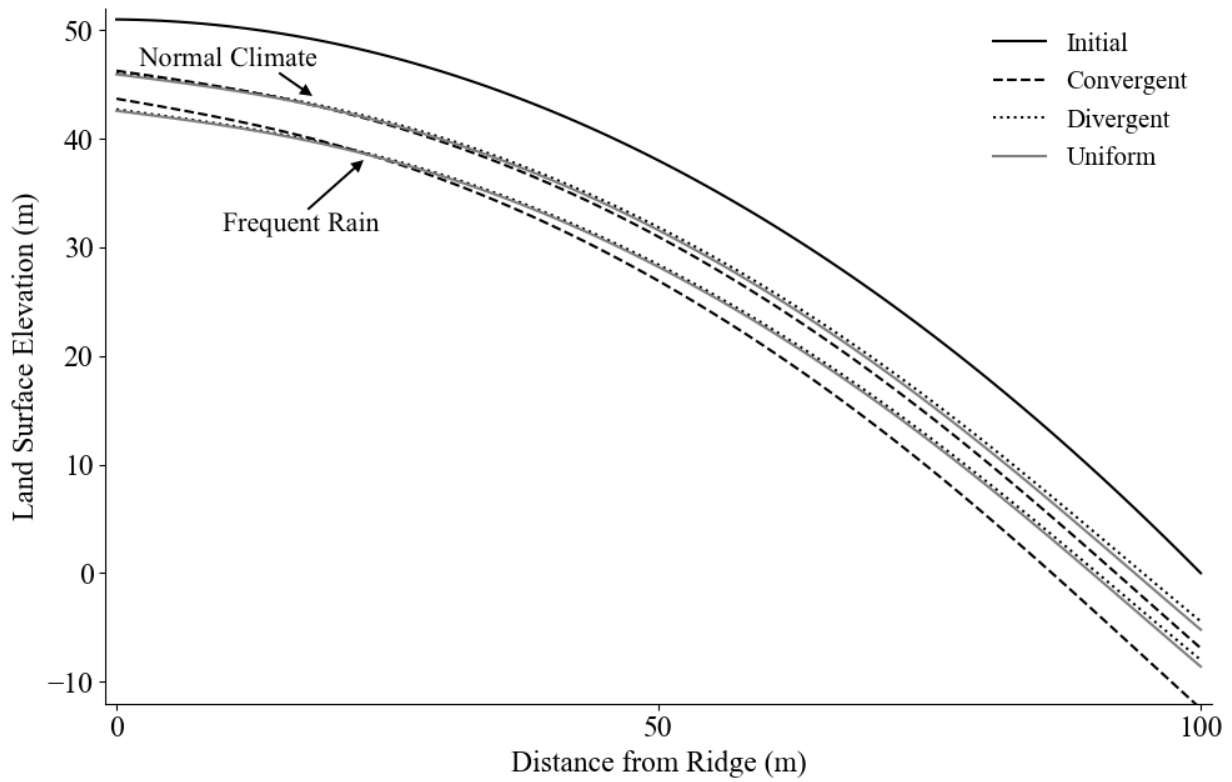
magnitude. Regardless, the evolutionary behavior of convergent convex hillslopes still indicates a positive feedback loop mechanism.

Figure 15 shows the evolution of a concave hillslope over 10,000 years. Two simulations with different convergence rates are shown. On the concave hillslope there is little apparent difference in the evolution of convergent hillslopes with different values of  $c$ . The concave hillslope acts almost oppositely to the convex hillslope; the differences in convergence rates are only manifested in the evolution of the divergent hillslopes, with the convergence rate of greater magnitude on the divergent hillslope resulting in less chemical erosion. This indicates a positive feedback as well, but the feedback mechanism on the divergent hillslopes operates in a subtractive manner. If on either side of a divergent section of hillslope the hillslope is convergent (as is shown in the center of Figure 1a), then we might expect hillslope evolution to cause deepening of the convergent

hillslopes, which, in addition to making the convergent sections more convergent, might make the divergent section more divergent. The resultant more-divergent hillslope would, as Figure 15 demonstrates, experience less chemical erosion than before, allowing this section of hillslope to become even more divergent as convergent sections around it are lowered. We see again that hillslope planform can exert significant control over chemical erosion rates and hillslope evolution. When convergent rates are of larger magnitude, diffusive hillslope processes are less able to smooth the varied topography created by chemical erosion. If chemical erosion rates are high enough, a positive feedback mechanism caused by chemical erosion can cause further lowering of already lowered sections of hillslope and limit the lowering of already less-eroded hillslope sections.

#### 6.2.4 Varying Rainstorm Frequency and Intensity

Figure 16 shows the evolution of a convex hillslope subject to both soil diffusion and chemical erosion over 10,000 years. Two simulations are shown, one with a "normal" climate and one with a "frequent rain" climate. In both simulations, the net annual precipitation is equal and thus the total water reaching the two hillslopes over 10,000 years is equal. The hillslope subjected to a "normal" climate has less frequent rainstorms of greater intensity while the hillslope subjected to a "frequent rain" climate has more frequent rainstorms of lesser intensity. Note that for the "frequent rain" climate, as for the "normal" climate, parameters are chosen such that the water table dries completely between successive storms. It is remarkable that rainstorm frequency and intensity seems to exert significant control over total chemical denudation and thus hillslope evolution. A climate with more frequent, less intense, rainstorms causes a greater amount of total chemical erosion. This is due to the nonlinear behavior of the perched water table flow. The perched water table approaches a steady state as it rains. That means that as the water table rises, the rate at which it rises decreases. Thus, exposure time does not increase additively with rainstorm intensity and the rate of increase in exposure time, and total chemical denudation, decreases with increasing rainstorm intensity and growing water table height. The hillslope that experiences more frequent but less intense rainstorms will have a greater annual exposure time, even though the exposure from a single storm is lesser. Thus the hillslope experiencing the "frequent rain" climate experiences a greater amount of chemical erosion. This behavior indicates a complex and unexpected



**Figure 16:** Hillslope evolution with soil diffusion and chemical erosion. Varying rainstorm frequency and intensity with a “normal” climate defined by three hour storms of intensity one cm per hour and 104 storms per year and a “frequent rain” climate defined by three hour storms of intensity 0.25 cm per hour and 416 storms per year. Convex hillslope, 10,000 year simulation,  $D = 0.01 \text{ m}^2 \text{ yr}^{-1}$ ,  $c = 0.2$ , and  $R_{dis} = 2 \times 10^{-9} \text{ mol m}^2 \text{ s}^{-1}$ . Resultant chemical denudation rates when averaged over the planforms are approximately  $5 \times 10^{-4}$  and  $9 \times 10^{-4} \text{ m yr}^{-1}$ , respectively, with denudation ratios averaged over the planforms approximately 0.90 and 0.94.

link between climate and hillslope evolution.

#### 6.2.5 Varying Diffusivity, Hillslope Evolution Over Longer Timescales

The simulations we have discussed indicate that under conditions of strong chemical denudation rates, a positive feedback mechanism may exist and contribute diversity to hillslope topography. These results provides an explanation for why hillslopes might evolve into varied configurations when mechanical-diffusive processes create smooth hillslope forms and decrease topographic diversity. A major caveat to this conclusion is that the chemical erosion rates that do instigate a positive feedback mechanism are relatively large. Note, however, that all of our simulations thus far have maintained a constant diffusivity of  $D = 0.01$ . A range of diffusivity constants has been

reported in the literature (Section 5.1), however, and many are smaller than our chosen value. Perhaps a hillslope characterized by a smaller diffusivity would evolve in the varied manner induced by relatively strong chemical denudation, even when chemical denudation rates are relatively weak. We turn to our low chemical erosion rates, which are on the order of  $5 \times 10^{-5}$ , and run simulations with a smaller diffusivity,  $D = 0.001$ . Our initial attempts at running these simulations over 10,000 years produce figures that erode so little that distinguishing between the lines in the figures is impossible. Thus, we run these simulations over 100,000 years, despite some major caveats to doing so. Hillslope evolution might occur with some consistency over 100,000 years, but this timescale could also include, for example, a full glacier cycle. Major shifts in environmental conditions could completely alter patterns of erosion such that these simulations are unrealistic. Regardless, we are still interested in seeing if the principle of positive feedback caused by chemical erosion is plausible, and so we run the simulations as described.

Figure 17 shows the evolution of a convex hillslope over 100,000 years. Two simulations are shown, one run with  $D = 0.01$  and one run with  $D = 0.001$ . The hillslope evolution simulation with the higher diffusivity, as we might expect, evolves into the form of a straight line, with few spatially consistent differences in erosion between the convergent, uniform, and divergent hillslopes. The simulation does show that the convergent hillslope erodes further downslope but the divergent hillslopes erodes further upslope. This complex behavior does not seem to indicate any positive feedback mechanism. The simulation with the lower diffusivity shows significant and spatially consistent differences between all of the hillslopes, with the convergent hillslope eroding the most and the divergent hillslope eroding the least (these results are similar to those presented in Figure 12). We conclude that a chemical erosion positive feedback may occur if chemical erosion rates are strong enough to create topographic variety at rates that diffusion of soil cannot smooth out. Conversely, the principle of the positive feedback is maintained if diffusion of soil is too weak to smooth out the topographic variety created by chemical erosion.

### 6.3 Addressing Assumptions

This paper has combined a fluid dynamical model for subsurface flow on a hillslope and a number of geomorphological models for hillslope evolution. Many assumptions went into the development of our holistic model, which is the first (to the best of our knowledge) to account for both

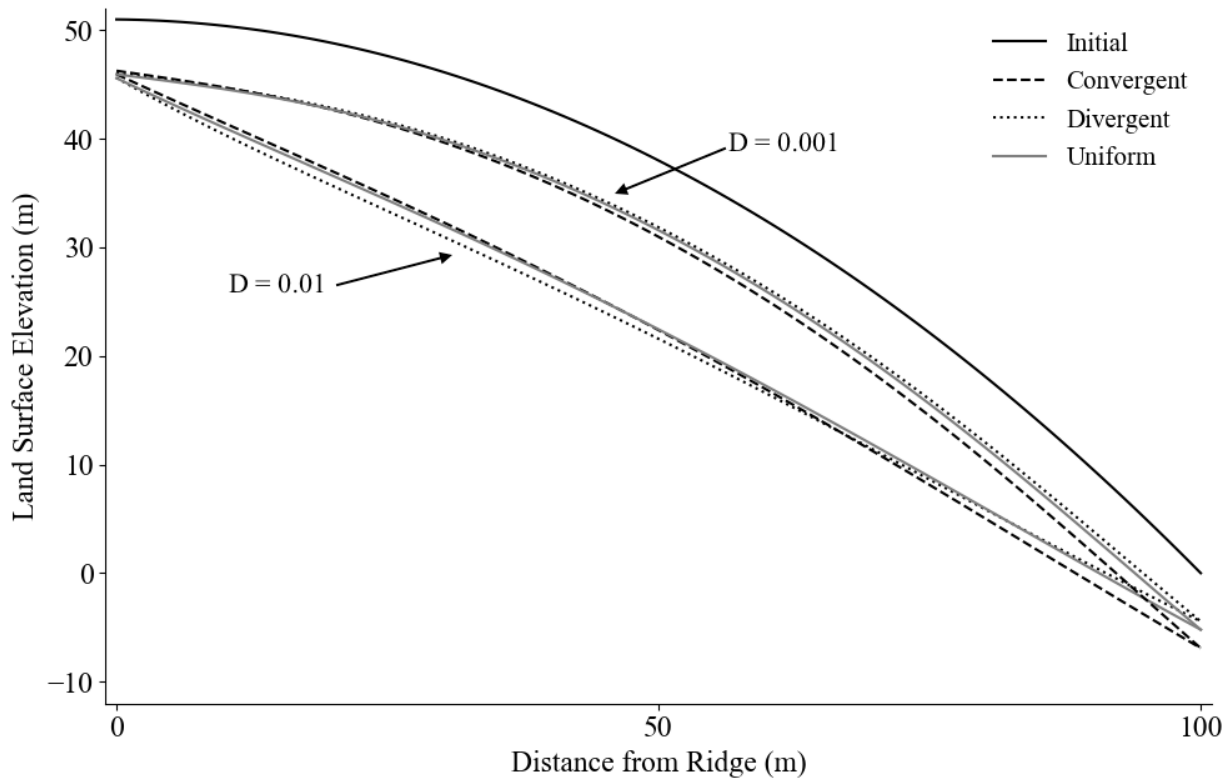


**Figure 17:** Hillslope evolution with soil diffusion and chemical erosion. Varying diffusivity from 0.01 to 0.001. Convex hillslope, 100,000 year simulation,  $R_{dis} = 2 \times 10^{-10}$  mol m $^2$  s $^{-1}$ ,  $N = 0.009$  m hr $^{-1}$ , 104 storms per year. Resultant chemical denudation rates for both simulations, when averaged over the planforms, are approximately  $5 \times 10^{-5}$  m yr $^{-1}$  with denudation ratios, when averaged over the planforms, of approximately 0.54 for the simulation with  $D = 0.01$  m $^2$  yr $^{-1}$  and 0.9 for the simulation with  $D = 0.001$ .

dynamic chemical and mechanical denudation, and it is appropriate to address these assumptions and the problems they pose. Our basic hillslope definition assumes that a hill consists of a soil mantle that overlies saprolite, which in turn overlies bedrock. In many locales there is little or no saprolite overlying bedrock, however, this does not pose much of a problem for our model. We might still expect a perched water table to form over the bedrock layer and we may even be able to extend our model for chemical erosion to account for chemical erosion at a soil-bedrock interface. We also assume, as do many other studies in the field of hydrogeology, that hydraulic conductivity and drainable porosity of soil and hydraulic conductivity saprolite are spatially uniform.

Some of the major assumptions we make pertain to the kinematic wave approximation for subsurface flow. The kinematic wave approximation ignores capillary forces exerted on water in the subsurface. Our model similarly ignores the chemical effects of water in the unsaturated zone.

Hydrological studies indicate that in relatively humid climates, even after a perched water table drains, water remains in the pores of subsurface material (unsaturated water content). This water might dissolve, or even precipitate, minerals after the perched water table disappears. It is more likely, however, that this small amount water quickly becomes saturated and thus does not have as significant a control on chemical erosion in the subsurface as does the more extensive volume of water that flows beneath the perched water table in response to rain storms. Additionally, our description of hillslope hydrology is applicable primarily to humid, forested environments with thick soil mantles. In a desert, for example, Hortonian overland flow is common and the overland flow of water may exert significant control over the mechanical transport of sediment at the surface. Only in environments where essentially all rainwater infiltrates into the subsurface could our model be applied. This assumption is common to many geomorphological studies, however, and many of the classic locales for the study of hillslope evolution, including the Appalachian Mountains and Oregon Coast Range, satisfy this requirement. It is also worth mentioning that our model should not be applied in karst regions, where calcium carbonate is present in the bedrock and the impacts of hydrologic flow in the subsurface are highly erosive and unpredictable.

Assumptions pertaining to the geomorphological aspects of this study include that the soil mantle is only physically mobile and the saprolite only chemically mobile. Almost certainly, subsurface flow can dissolve minerals within the soil column and can also precipitate minerals into the soil column; the erosion of the soil is not truly limited to mechanical processes. Similarly, there are mechanical processes that disturb both saprolite and bedrock, including freeze-thaw cycles and bioturbation by critters and plant-root growth. The assumption that saprolite is only subject to chemical erosion is likely false, although perhaps a reasonable estimation. Another limitation of our model is the fact that we do not account for chemical processes occurring in or around the bedrock. We have mentioned studies that have shown that perhaps half of the mass flux away from a hillslope is due to chemical processes, but much of this chemical loss occurs during the conversion of bedrock to saprolite. The chemical losses during the conversion from saprolite to soil are less clear. Our model might be better formulated with chemical denudation representing the loss of mass from the bedrock rather than loss of mass from the saprolite, however we expect that this would not make a large difference in the simulation results.

Our chosen annual storm ensemble also makes implicit assumptions. We assumed that rain-

storms occur equally spaced in time and last consistent lengths of time. In reality, rainstorms act in no comparably consistent manner and on real hillslopes, a perched water table may still exist above the soil-saprolite interface when another rainstorm occurs. It is also worth noting that, in reference to simulations varying rainstorm frequency and intensity, climate can change significantly over 10,000 years. Although rainstorm patterns apparently exert important influence on hillslope evolution, it may not be a safe assumption that chemical erosion acts consistently over geomorphic timescales.

One of the more significant problems with our model is that we only account for erosion that occurs deterministically; the linear soil diffusion and chemical denudation models describe denudation as a result of processes that remain uniform through time. We ignore more random processes like bedrock fracturing and landsliding. Indeed, it seems plausible that bedrock fracturing (Lebedeva and Brantley, 2017) and landsliding could significantly impact hillslope evolution. Bedrock fracturing in particular could interact in complex ways with subsurface flow. A bedrock fracture might preferentially channel subsurface flow and experience significantly more chemical erosion than other parts of the hillslope. Assumptions aside, our novel attempt at examining the impact of chemical erosion on hillslope geomorphology has provided us with insight into the mechanisms that create the diverse hillslope geometries observed in the field that mechanical mechanisms have failed to explain.

## 7 Conclusion: Implications for Hillslope Evolution

Our unique model for hillslope evolution, though highly simplified and applicable to an arguably narrow range of environments, provides an interesting look at how chemical erosion may impact the evolution of hillslopes. Our simulations indicate that chemical denudation can impact hillslopes in ways that widely differ from established mechanical models of hillslope evolution. In environments where chemical erosion is strong, hillslopes may evolve into varied forms with swale-like geometries that are distinct from the smooth geometries predicted by purely mechanical models of hillslope evolution. Already lowered sections of hillslope may preferentially erode lower due to convergent subsurface hydrologic flow and non-lowered sections of hillslope may erode less due to divergent hydrologic flow. A positive feedback of chemical erosion due to subsurface hydrology is plausible and this mechanism is particularly sensitive to the planform of a given section of hillslope. Convergence rates of greater magnitude increase the strength of the chemical erosion in convergent swales and decrease the strength of chemical erosion in divergent swales. The positive feedback mechanism is more likely to operate when soil creep diffusivity is low, chemical erosion rates are high, and rainstorms occur frequently.

The effects of chemical denudation are sensitive to the concavity of the hillslope in addition to the planform. On concave hillslopes, subsurface flow gathers at the bottom of the hill for greater lengths of time and so the differences in long-term chemical denudation between convergent and divergent concave hillslopes are smaller than the differences between convergent and divergent convex hillslopes, although even concave hillslopes may exhibit the positive feedback mechanism. Due to the nonlinear behavior of subsurface perched water table flow, hillslope chemical denudation is particularly sensitive to rainstorm frequency and intensity; hillslopes subjected to climates with frequent rainstorms may be impacted more by chemical denudation than hillslopes subjected to climates with infrequent rainstorms, even when the total amount of rain is held constant.

The implications of this study might be examined in greater detail. It would be interesting to see how the impacts of chemical erosion on hillslope evolution vary over longer timescales, particularly in the face of changing climate, which can certainly vary significantly over timescales on the order of  $10^4$  years . Following Furbish and Fagherazzi (2001), a complete stability analysis of the chemical denudation problem might be performed to examine whether the positive feedback

mechanism observed here may cause hillslope evolution to proceed in a truly unstable manner. Different models of hydrologic flow could be used to estimate chemical denudation, particularly models that are more complex and accurate than the kinematic wave approximation (although using these would rule out using analytical solutions to solve the perched water table flow problem). Our initial exploration reveals that chemical denudation may indeed act as a positive feedback mechanism and may be responsible for diverse hillslope geometries and swale topographies. Chemical erosion likely contributes to the variety of complex hillslope forms observed in the real world and further studies in the field of hillslope geomorphology should consider the possible impacts of chemical processes.

## 8 References

- Anderson, Suzanne and Anderson, Robert. *Geomorphology: the mechanics and chemistry of landscapes.* Cambridge University Press. 2010.
- Anderson, Suzanne P, Blanckenburg, Friedhelm von, White, Arthur F. Physical and Chemical Controls on the Critical Zone. *Elements*, Vol. 3. 2007.
- Bevin, Keith. Kinematic subsurface stormflow. *Water Resources Research*, Vol. 17, No. 5. 1981.
- Buss, H.L., Sak, P.B., Webb, S.M., Brantley, S.L. Weathering of the Rio Blanco quartz diorite, Luquillo Mountains, Puerto Rico: coupling oxidation, dissolution, and fracturing. *Geochimica et Cosmochimica Acta* 72. 2008
- Casey, W.H., Holdren, G.R. Dissolution rates of plagioclase at pH = 2 and 3. *American Mineralogist*, Vol. 76. 1991.
- Chen, Yuan, Brantley, Susan L. Temperature and pH-dependence of albite dissolution rate at acid pH. *Chemical Geology*, Vol. 135. 1997.
- Culling, W.E.H. Analytical theory of erosion. *The Journal of Geology*, Vol. 68, No. 3. 1960.
- Dietrich, William E, Bellugi, Dino G, Sklar, Leonard S, Stock, Jonathan D. Geomorphic transport laws for predicting landscape form and dynamics. *Prediction in Geomorphology*. 2003.
- Dixon, J., Heimsatch, A., Amundson, R. The critical role of climate and saprolite weathering in landscape evolution. *Earth Surface Processes and Landforms*, Vol 34. 2009.
- Dixon, J. and Riebe, C. Tracing and pacing soil across slopes. *Elements*. October 2014.
- Doane, T. H., Furbish, D. J., Roering, J. J., Schumer, R., and Morgan, D. J. Nonlocal sediment transport on steep lateral moraines, eastern Sierra Nevada, California, USA. *Journal of Geophysical Research: Earth Surface*, Vol. 123. 2018.
- Dunne, Thomas and Leopold, Luna B. *Water in Environmental Planning*. W.H. Freeman. 1978.
- Fan, Y. and Bras, R. L. Analytical solutions to hillslope subsurface storm flow and saturation overland flow. *Water Resources Research*, Vol. 34, 921-927. 1998.
- Fernandes, N.F. and Dietrich, W.E. Hillslope evolution by diffusive processes: The timescale for equilibrium adjustments. *Water Resources Research*, Vol. 33. 1997
- Ferrier, K. et al. Mineral-specific chemical weathering rates over millennial timescales: Measurements at Rio Icacos, Puerto Rico. *Chemical Geology*, Vol. 277. 2010.
- Foufoula-Georgiou, E. , Ganti, V., and Dietrich, W. E. Dietrich. A nonlocal theory of sediment transport on hillslopes. *Journal of Geophysical Research*, Vol. 115. 2010.
- Furbish, D.J. and Fagherazzi, S. Stability of creeping soil and implications for hillslope evolution. *Water Resources Research*, Vol. 37. October 2001.
- Furbish, D. J., and P. K. Haff. From divots to swales: Hillslope sediment transport across divers length scales. *Journal of Geophysical Research*, Vol. 115. 2010.
- Furbish, D. J., and J. J. Roering. Sediment disentrainment and the concept of local versus nonlocal transport on hillslopes. *Journal of Geophysical Research: Earth Surface*, Vol. 118. 2013.
- Girdez, J.V. and Woolhiser, D.A. Analytical integration of the kinematic equation for runoff on a place under constant rainfall rate and Smith and Parlange infiltration. *Water Resources Research*, Vol. 32. November 1996.
- Hanks, T. C., Bucknam, R. C., Lajoie, K. R., and Wallace, R. E. Modification of wave-cut and faulting-controlled landforms. *Journal of Geophysical Research*, Vol. 89. 1984.
- Henderson, F.M. and Wooding, R.A. Overland flow and groundwater flow from a steady rainfall of finite duration. *Journal of Geophysical Research*, Vol. 69. 1964.

- Jin, L et al. Mineral weathering and elemental transport during hillslope evolution at the Susquehanna/Shale Hills Critical Zone Observatory. *Geochimica et Cosmochimica Acta* 74. 2010.
- Jin, L and Brantley, S.L. Soil chemistry and shale weathering on a hillslope influenced by convergent hydrologic flow regime at the Susquehanna/Shale Hills Critical Zone Observatory. *Applied Geochemistry*, Vol. 26. 2011.
- Kirkby, M.J. Hillslope process-response models based on the continuity equation. 1971.
- Lebedeva, M.I. and Brantley, S.L. Weathering and erosion of fractured bedrock systems. *Earth Surface Processes and Landforms*. 2017.
- Li, Yuan-Hui. Denudation of Taiwan Island since the Pliocene Epoch. *Geology*. February 1976.
- Logan, J.D. *Applied Mathematics: A Contemporary Approach*. John Wiley, New York. 1987.
- Maher, K. The dependence of chemical weathering rates on fluid residence time. *Earth and Planetary Science Letters*, Vol. 294. 2010.
- Matmon, A., Bierman, P., Larsen, J., Southworth, J., Pavich, M., and Caffee, M. Temporally and spatially uniform rates of erosion in the southern appalachian great smoky mountains, *Geology*, Vol. 31. 2003.
- McKean, J. A., Dietrich, W. E., Finkel, R. C., Southon, J. R. and Caffee, M. W. Quantification of soil production and downslope creep rates from cosmogenic  $^{10}\text{Be}$  accumulations on a hillslope profile. *Geology*, Vol. 21. 1993.
- Mudd, S. and Furbish, D. J. Influence of chemical denudation on hillslope morphology. *Journal of Geophysical Research*, Vol. 109. 2004.
- Nash, D., Morphologic dating of degraded normal fault scarps. *Journal of Geology*, Vol. 88. 1980b.
- Reneau, S . L., Depositional and erosional history of hollows: application to landslide location and frequency, long-term erosion rates, and the effects of climatic change, Ph.D. dissertation, University of California, Berkeley. 1988.
- Roering, Joshua J. Evidence for nonlinear, diffusive sediment transport on hillslopes and implications for landscape morphology. *Water Resources Research*, Vol. 35, No. 3. 1999.
- Roering, J. J., Perron, J. T., and Kirchner, J. W. Functional relationships between denudation and hillslope form and relief, *Earth and Planetary Science Letters*, Vol. 264. 2007.
- Scanlon, Todd M, Clapp, Roger B. Shallow subsurface storm flow in a forested headwater catchment: Observations and modeling using a modified TOPMODEL. *Water Resources Research*, Vol. 36, No. 9. 2000.
- Sloan, P.G. and Moore, I.D. Modeling subsurface stormflow on steeply sloping forested watersheds. *Water Resources Research*, Vol. 20. December 1984.
- Troch, P. et al. Analytical solutions to a hillslope-storage kinematic wave equation for subsurface flow. *Advances in Water Resources*, Vol. 25. February 2002.
- Turner, B.F., Stallard, R.F., Brantley, S.L. Investigation of in situ weathering of quartz diorite bedrock in the Rio Icacos basin, Luquillo Experimental Forest, Puerto Rico. *Chemical Geology*, Vol. 202. 2003.
- USDA Forest Service. El Yunque National Forest, Fire and Aviation. Accessed at [https://www.fs.usda.gov/detail/elyunque/home/?cid=fsbdev3\\_043024](https://www.fs.usda.gov/detail/elyunque/home/?cid=fsbdev3_043024) on March 3, 2018.
- Velbel, Michael A. Geochemical mass balances and weathering rates in forested watersheds of the southern blue ride. *American Journal of Science*, Vol. 285. 1985.
- Vepraskas, M.J., Guertal, W.R., Kleiss, H.J., and Amoozegar, A. Porosity factors that control the hydraulic conductivity of soil-saprolite transitional zones. *Soil Science Society of America Journal* Vol. 60. 1996.
- Welch, S.A., Ullman, W.J. The effect of organic acids on plagioclase dissolution rates and stoichiometry. *Geochimica et Cosmochimica Acta*, Vol. 57. 1993.

White, A.F., Brantley, S.L. The effect of time on the weathering of silicate minerals: why do weathering rates differ in the laboratory and field? *Chemical Geology*, Vol. 202. 2003.

## 9 Supplemental Material

### 9.1 Method of Characteristics for Perched Water Table Flow

The following equation is the kinematic approximation for perched water table flow.

$$\frac{\partial h}{\partial t} - K(\beta + 2\alpha x) \frac{\partial h}{\partial x} = N + Kh \frac{c\beta + 4\alpha cx + 2\alpha b_0}{(b_0 + cx)}. \quad (44)$$

Equation 44 is a quasi-linear wave equation (Logan, 1987), a partial differential equation in the form of a wave equation with a source/sink term (the right side of equation 44) and a non-constant wave speed (the coefficient  $-K(\beta + 2\alpha x)$ ). If  $N$  is constant, equation 44 can be solved with the method of characteristics, which splits the equation into two ordinary differential equations (Logan, 1987; Fan and Bras, 1998; Troch et al., 2002),

$$\frac{dx}{dt} = -K(\beta + 2\alpha x), \quad (45)$$

which describes a family of characteristic curves in the  $x$  -  $t$  plane, and

$$\frac{dh}{dx} = -\frac{N}{K(\beta + 2\alpha x)} - h(x, t) \frac{c\beta + 4\alpha cx + 2\alpha b_0}{(b_0 + cx)(\beta + 2\alpha x)}, \quad (46)$$

which describes how the perched water table propagates along these curves (Fan and Bras, 1998; Troch et al., 2002). For the planar hillslope, where  $\alpha = 0$ , the two equations simplify to

$$\frac{dx}{dt} = -\beta K, \quad (47)$$

and

$$\frac{dh}{dx} = -\frac{N}{\beta K} - h(x, t) \frac{c\beta}{\beta(b_0 + cx)}. \quad (48)$$

We wish to solve the two pairs of ordinary differential equations above so that we can describe perched water table flow on both planar and parabolic hillslopes.

### 9.1.1 Analytical Solutions to the Kinematic Wave Equation, Planar Hillslope

Equations 47 and 48 have solutions:

$$x(t) = C_1 - K\beta t \quad (49)$$

and

$$h(x) = -\frac{N(b_0x + \frac{1}{2}cx^2)}{K\beta(b_0 + cx)} + \frac{C_2}{(b_0 + cx)}. \quad (50)$$

The two constants of integration can now be solved on multiple  $x - t$  domains, allowing the geometry of the perched water table to be calculated analytically for both the rising limb, when it is raining and the perched water table is rising, and for the decaying limb, when rain ceases and the perched water table drains. To do this, we break the  $x - t$  domain into four distinct regions (Figure 6).

Imagine that as the water table rises, there are particles of water that we can track in a Lagrangian manner. Only particles that leave from the  $x$  domain, from  $x = 0$  to  $x = L$ , enter our water table. At the beginning of a rainstorm, we assume that there is no existing perched water table. As it rains, the perched water table grows in height at all values of  $x$ . By the end of a rainstorm of realistic length, the water table will reach a state of partial equilibrium (Troch et al., 2002). Partial equilibrium, as its name implies, describes a state where only part of the water table has reached steady state conditions. The steady state condition of the perched water table is defined by the motion of a characteristic (imaginary) fluid particle that leaves from  $x = 0$ . Equation 49 above describes the  $x$  position of characteristic particles. The constant of integration is solved based on which particle we wish to examine. Here, we wish to examine the characteristic particle leaving from  $x = 0$  at time  $t = 0$ . We see then that our constant of integration,  $C_1$ , solves to 0. We can use this resultant equation to find the  $x$ -position of the characteristic particle leaving from  $x = 0$  at any time  $t$ . Once that characteristic particle leaves the  $x$ -domain of our hillslope ( $[0, L]$ ), the water table (at least over the domain of our hillslope) has reached equilibrium. Examine the solution to equation 49 for the characteristic particle leaving from  $x = 0$  at  $t = 0$ :

$$x(t) = -K\beta t. \quad (51)$$

Using the  $\beta$  value for our convex hillslope (Table 1), -1.01, and a hydraulic conductivity value of

$3.6 \text{ m hr}^{-1}$ , we can determine how long it takes for the characteristic particle to travel to the  $x$  position  $L = 200$ , which is how long it takes for the water table to reach steady state. We find that it takes about 55 hours of continuous rain for the water table to reach steady state. We assume that we never have a storm of such magnitude on our hillslopes and so must calculate the geometry of the perched water table in its partially equilibrated state. We define  $x_{crit}$  as the distance  $x$  that the characteristic particle leaving from  $x = 0$  travels after the length of a rainstorm,  $T_R$ . If  $x_{crit} > L$  then the perched water table has reached steady state, if  $x_{crit} < L$  then the perched water table has reached only partial equilibrium. For the planar hillslope,

$$x_{crit} = -K\beta T_R. \quad (52)$$

To find the perched water table after a given rainstorm of length  $T_R$  in a partially equilibrated state, we solve equations 49 and 50 over two  $x$  domains,  $x = [0, x_{crit}]$  and  $x = [x_{crit}, L]$ . These are the Domains 1 and 2 (Figure 6). Within the Domains 1 and 2,  $N$  is the constant rainfall rate minus the infiltration rate of water into the saprolite (the hydraulic conductivity of the saprolite), which we simply label  $N$ . After the rainstorm ends, the perched water table flows downslope and drains into the saprolite simultaneously. During this decay phase, the characteristic particle continues to flow downslope. Thus we must also describe the decay phase over two separate domains, Domains 3 and 4 (Figure 6). Within Domains 3 and 4,  $N$  is equal to just the infiltration rate of water into the saprolite, which we label  $N_D$ .

Thus we must describe the perched water table over four domains in the  $x - t$  plane. We assume that at  $t = 0$  it begins to rain on a hillslope that has no perched water table formed,  $h = 0$ . It rains until time  $t = T_R$  and the water table begins to drain. We find the perched water table as it rises with Domain 1 and Domain 2 and as it drains with Domain 3 and Domain 4.

**Domain 1** Domain 1 is bounded by  $t = 0$ ,  $t = T_R$ ,  $x = L$ , and  $t = t(x, \epsilon) = t(x, 0)$ , where  $\epsilon$  represents a characteristic particle leaving from every value of  $x$  and due to our boundary condition,  $\epsilon = 0$ . Boundary and Initial Conditions

$$t(\epsilon) = 0, \quad h(\epsilon) = 0 \quad (53)$$

result in the solutions

$$x = \epsilon - K\beta t \quad (54)$$

and

$$h(x) = \frac{N}{\beta K(b_0 + cx)} \left( b_0(\epsilon - x) + \frac{1}{2}c(\epsilon^2 - x^2) \right) \quad (55)$$

which are solved at a chosen time  $T_R$ , the length of the rainstorm after which we wish to observe the perched water table, and over the domain  $\epsilon = [0, L]$ .

**Domain 2** Domain 2 is bounded by  $t = T_R$ ,  $x = 0$ , and  $t = t(x, 0)$ . Boundary and initial conditions

$$t(0) = \tau, \quad h(0, t) = 0 \quad (56)$$

result in the solutions

$$x = K\beta(\tau - t) \quad (57)$$

and

$$h(x) = -\frac{N(b_0x + \frac{1}{2}cx^2)}{K\beta(b_0 + cx)} \quad (58)$$

which are solved at a chosen time  $t = T_R$  and over the domain  $\tau = [0, T_R]$ . Equation 58 represents the steady state solution when plotted over the entire x domain.

**Domain 3** Domain 3 is bounded by  $t = T_R$ ,  $x = 0$ , and a characteristic curve passing through  $x_{crit}$ , which represents the x location of a characteristic particle that started at  $x = 0$  and  $t = 0$ . Boundary and initial conditions

$$t(x^*) = T_R, \quad h(x^*) = h(x^*, T_R) \quad (59)$$

result in the solutions

$$x = K\beta(T_R - t) + x^* \quad (60)$$

and

$$h(x) = \frac{N(b_0(x^* - x) + \frac{1}{2}c(x^{*2} - x^2))}{\beta K(b_0 + cx)} + \frac{h(x^*, T_R)(b_0 + cx^*)}{(b_0 + cx)} \quad (61)$$

which are solved at a chosen time  $t$ , where  $t > T_R$  and  $t - T_R = T_D$ , the amount of time since the rainfall stopped (and the water table has been draining), and over the domain  $x^* = [0, x_{crit}]$ . These solutions describe the decay of the section of perched water table between  $x = 0$  and  $x = x_{crit}$ .

**Domain 4** Domain 4 is bounded by  $t = T_r$ ,  $x = L$ , and a characteristic curve passing through  $x_{crit}$ . Boundary and initial conditions

$$t(x') = T_R, \quad h(x') = h(x', \epsilon) \quad (62)$$

result in the solutions

$$x = K\beta(T_R - t) + x' \quad (63)$$

and

$$h(x) = \frac{N(b_0(x' - x) + \frac{1}{2}c(x'^2 - x^2))}{\beta K(b_0 + cx)} + \frac{h(x', T_R)(b_0 + cx')}{(b_0 + cx)} \quad (64)$$

which are solved at a chosen time  $t$ , where  $t > T_R$ , and

over the domain  $x' = [x_{crit}, L]$ . These solutions describe the decay of the section of perched water table between  $x = x_{crit}$  and  $x = L$ .

### 9.1.2 Analytical Solutions to the Kinematic Wave Equation, Parabolic Hillslope

For the parabolic hillslopes we solve equations 45 and 46 following the steps above.

$$x(t) = C_1 e^{-\alpha K t} - \frac{\beta}{\alpha}. \quad (65)$$

and

$$h(x) = -\frac{N(b_0 x + \frac{1}{2}cx^2)}{K(\beta + \alpha x)(b_0 + cx)} + \frac{C_2}{(\beta + \alpha x)(b_0 + cx)}. \quad (66)$$

For the parabolic hillslopes,

$$x_{crit} = \frac{\beta}{\alpha} (e^{-\alpha K T_R} - 1). \quad (67)$$

### Domain 1

$$x = \left(\epsilon + \frac{\beta}{\alpha}\right) e^{-\alpha k t} - \frac{\beta}{\alpha} \quad (68)$$

and

$$h(x) = \frac{N}{K(\beta + \alpha x)(b_0 + cx)} \left( b_0(\epsilon - x) + \frac{1}{2}c(\epsilon^2 - x^2) \right) \quad (69)$$

### Domain 2

$$x = \frac{B}{\alpha} \left( e^{\alpha K(\tau-t)} - 1 \right) \quad (70)$$

and

$$h(x) = \frac{-N(b_0 x + \frac{1}{2}cx^2)}{K(\beta + \alpha x)(b_0 + cx)}. \quad (71)$$

### Domain 3

$$x = \left( x^* + \frac{\beta}{\alpha} \right) e^{\alpha K(T_R-t)} - \frac{\beta}{\alpha} \quad (72)$$

and

$$h(x) = \frac{N_D(b_0(x^* - x) + \frac{1}{2}c(x^{*2} - x^2))}{K(\beta + \alpha x)(b_0 + cx)} + h(x^*, T_R) \frac{(\beta + \alpha x^*)(b_0 + cx^*)}{K(\beta + \alpha x)(b_0 + cx)}. \quad (73)$$

### Domain 4

$$x = \left( x' + \frac{\beta}{\alpha} \right) e^{\alpha K(T_R-t)} - \frac{\beta}{\alpha} \quad (74)$$

and

$$h(x) = \frac{N_D(b_0(x' - x) + \frac{1}{2}c(x'^2 - x'^2))}{K(\beta + \alpha x)(b_0 + cx)} + h(x', T_R) \frac{(\beta + \alpha x')(b_0 + cx')}{K(\beta + \alpha x)(b_0 + cx)}. \quad (75)$$

#### 9.1.3 Calculating the Rise and Decay of a Perched Water Table

To calculate the rise of the perched water table we use the solutions for Domains 1 and 2. The water table rises between times  $t = 0$  and  $t = T_R$ . To find the water table after some rainstorm of length  $T_R$ , we plug our chosen  $T_R$  into equation 54 for the planar hillslope (equation 68 for the parabolic hillslope) along with the domain  $\epsilon = [0, L]$ . We then plug the resultant values, along with our  $\epsilon$  domain, into equation 55 (equation 69 for parabolic) to find the perched water table at  $x$  values greater than  $x_{crit}$ . This is the perched water table over Domain 1. To find the perched water table at  $x$  values less than  $x_{crit}$ , we plug the domain  $\tau = [0, T_R]$  with the value  $t = T_R$  into equation 57 (equation 70 for parabolic). We then plug the resultant values for  $x$  into equation 58 (equation 71 for parabolic). This is the perched water table over Domain 2. Domains 1 and 2 have provided us with two ranges of  $h$  values. Combining the two ranges provides us a complete

description of the water table at time  $t = T_r$ .

To calculate the decay of the perched water table we use the solutions for Domains 3 and 4. We select a time  $t$  where  $t > T_R$ .  $t - T_r = T_d$  where  $T_d$  is the length of time the perched water table has drained after the end of a rainstorm (that lasted  $T_r$ ). We plug our chosen  $t$  value along with the domain  $x^* = [0, X_{crit}]$  into equation 60 (72 for parabolic) to find a range of  $x$  values. We then plug this range of  $x$  values, along with the domain  $x^*$  into equation 61 (73 for parabolic) to find the perched water table at  $x$  values less than  $x_{crit}$  after the water table has drained for time  $T_d$ . This is the perched water table over Domain 3. To find the perched water table at  $x$  values greater than  $x_{crit}$  we plug the domain  $x' = [x_{crit}, L]$  along with our chosen  $t$  value into equation 63 (74 for parabolic), which returns a range of  $x$  values. We then plug this range of  $x$  values, along with the domain  $x'$  into equation 64 (75 for parabolic) to find the perched water table at  $x$  values greater than  $x_{crit}$  after the water table has drained for time  $T_d$ . This is the perched water table over Domain 4.

## 9.2 Hillslope Evolution Simulations

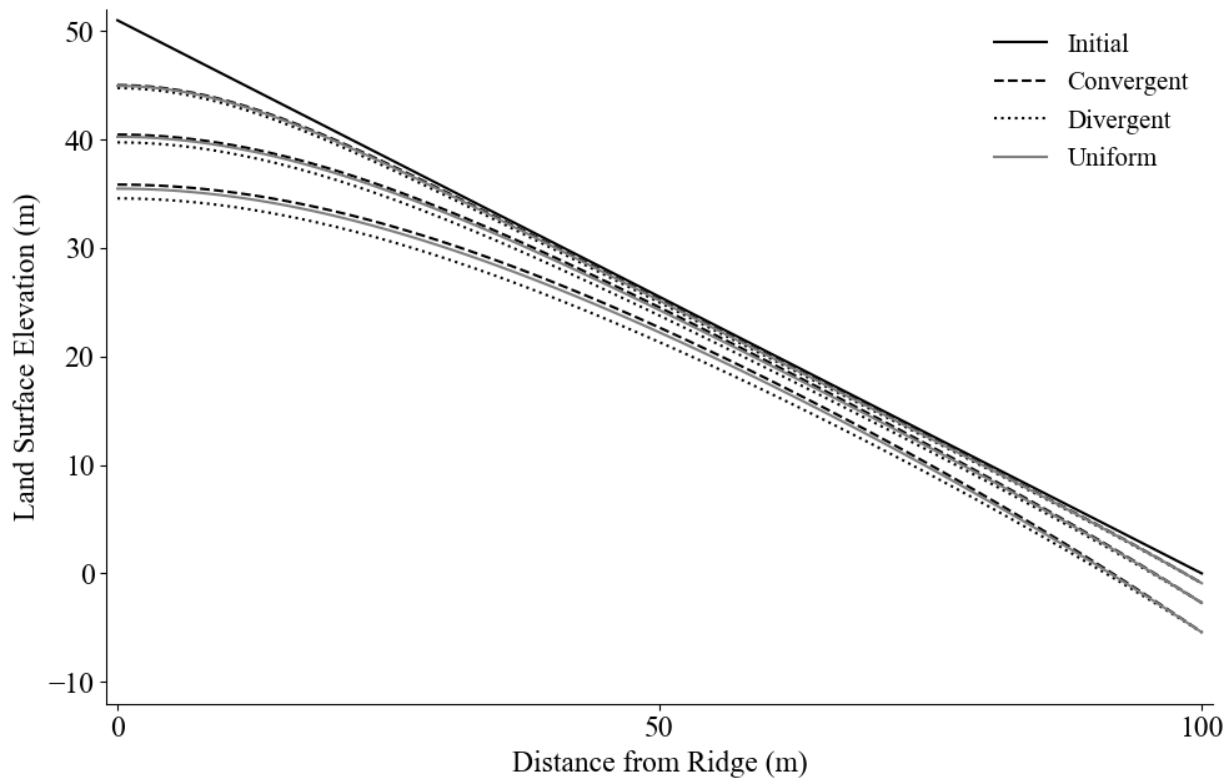


**Figure 18:** Hillslope evolution after 10,000, 30,000, and 60,000 years with mechanical soil diffusion only. Planar hillslope, 10,000 years simulation,  $D = 0.01 \text{ m}^2 \text{ yr}^{-1}$ .

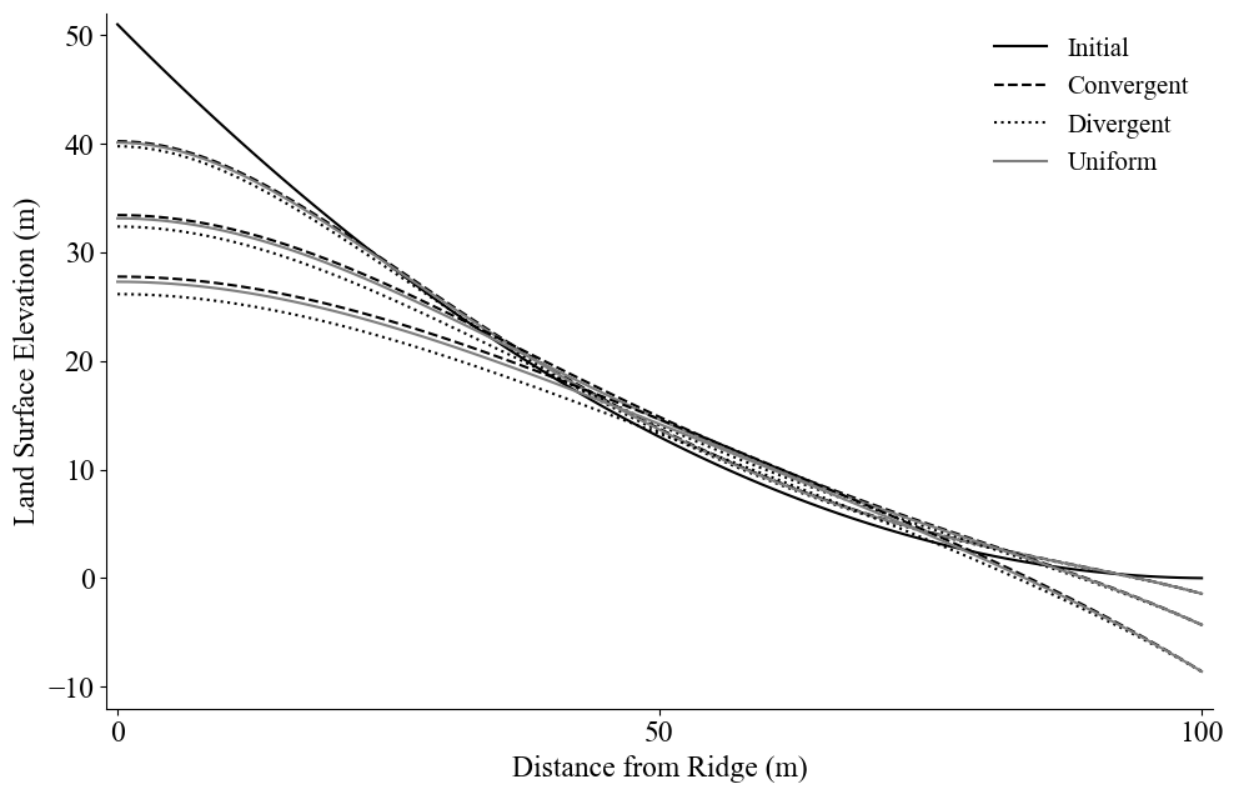


**Figure 19:** Hillslope evolution after 10,000, 30,000, and 60,000 years with mechanical soil diffusion only. Concave hillslope, 10,000 years simulation,  $D = 0.01 \text{ m}^2 \text{ yr}^{-1}$ .

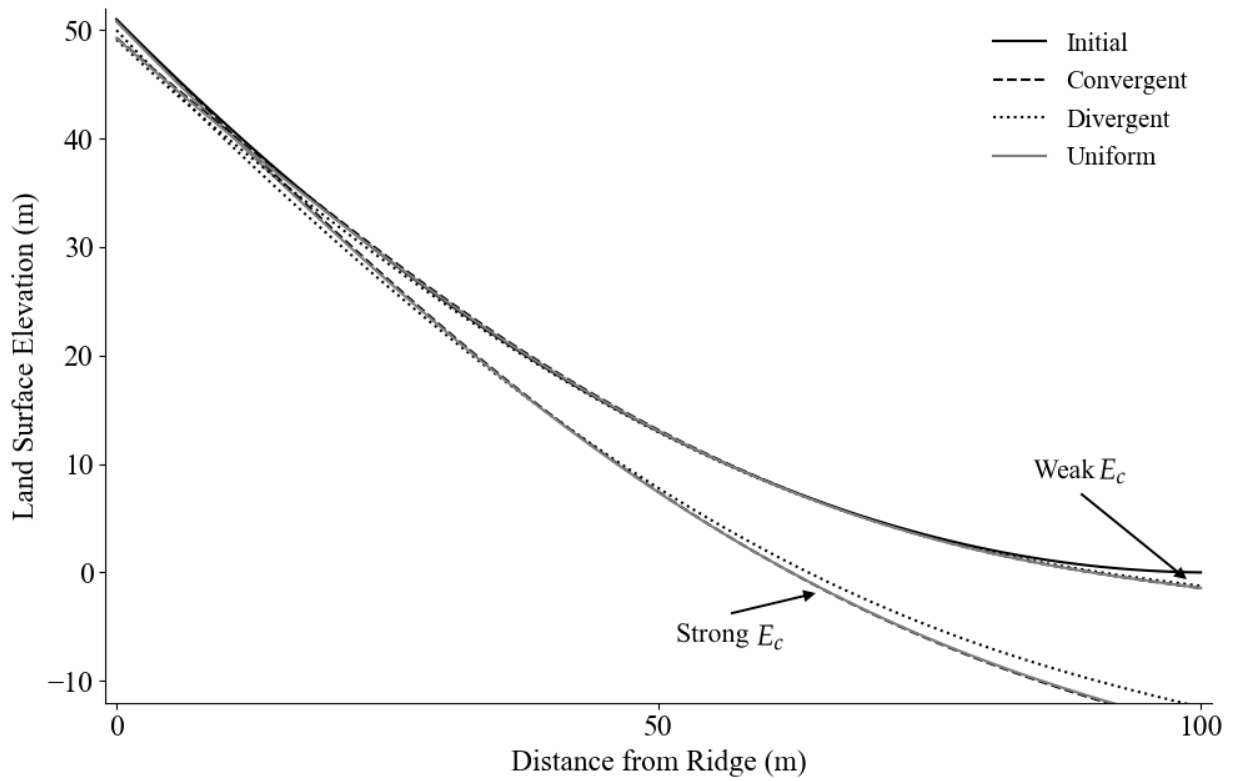


**Figure 20:** Hillslope evolution with soil diffusion and chemical erosion. Varying strength of chemical erosion with  $R_{dis} = 2 \times 10^{-9}$  mol  $\text{m}^{-2} \text{s}^{-1}$  and  $2 \times 10^{-10}$ . Concave hillslope, 10,000 year simulation,  $D = 0.01 \text{ m}^2 \text{ yr}^{-1}$ ,  $c = 0.2$ ,  $N = 0.009 \text{ m hr}^{-1}$ , 104 storms per year. Resultant chemical denudation rates when averaged over the planforms are approximately  $6 \times 10^{-4} \text{ m yr}^{-1}$  and  $6 \times 10^{-5}$ , respectively, with denudation ratios averaged over the planforms approximately 0.99 and 0.92.

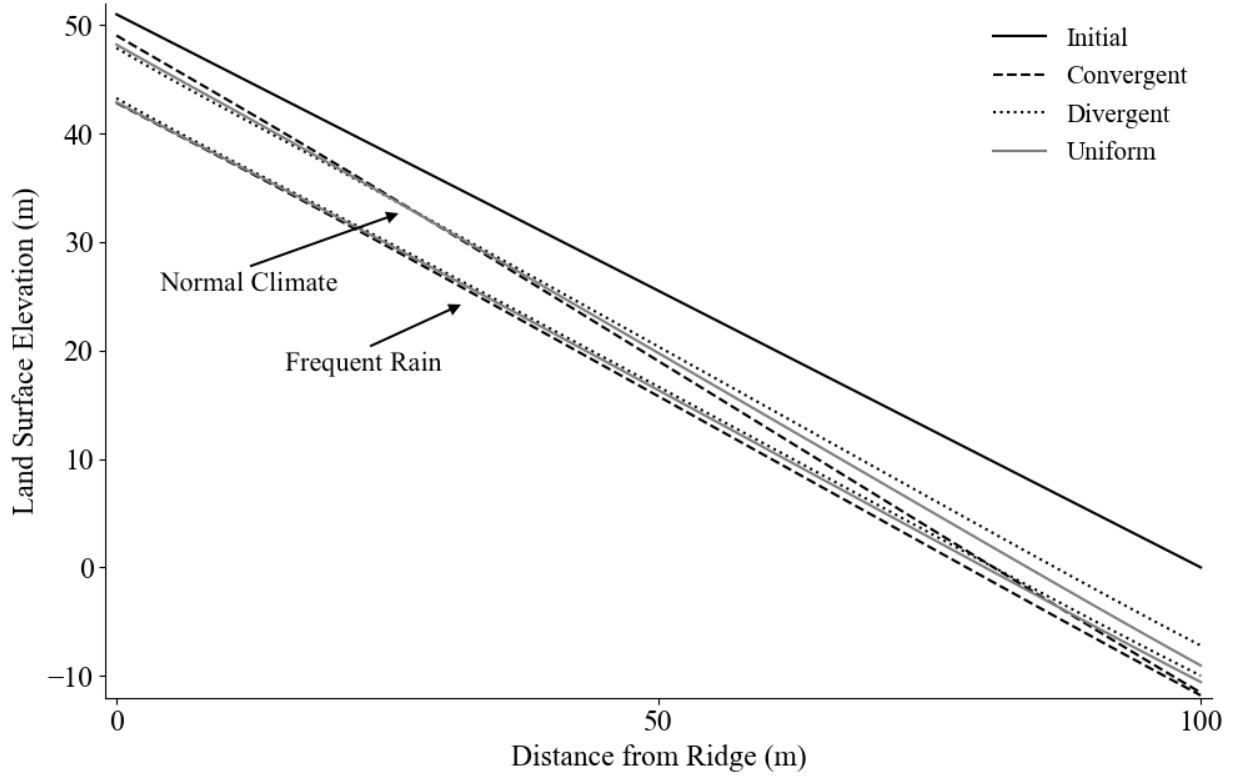


**Figure 21:** Hillslope evolution with soil diffusion and chemical erosion. Varying climate with a “normal” climate defined by three hour storms of intensity one cm per hour and 104 storms per year and a “frequent rain” climate defined by three hour storms of intensity 0.25 cm per hour and 416 storms per year. Planar hillslope, 10,000 year simulation,  $D = 0.01 \text{ m}^2 \text{ yr}^{-1}$ ,  $c = 0.2$ , and  $R_{dis} = 2 \times 10^{-9} \text{ mol m}^{-2} \text{ s}^{-1}$ . Resultant chemical denudation rates when averaged over the planforms are approximately  $5 \times 10^{-4} \text{ m yr}^{-1}$  and  $9 \times 10^{-4}$ , respectively, with denudation ratios averaged over the planforms approximately 0.94 and 0.97.

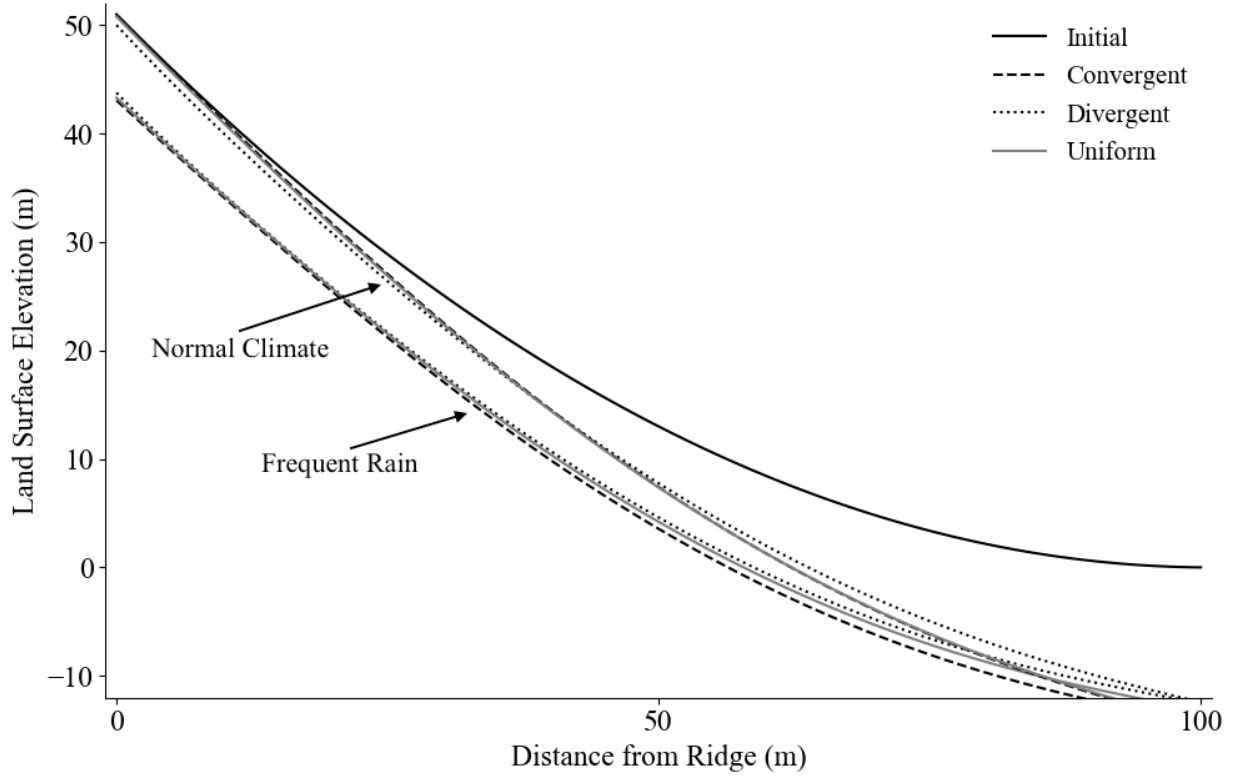


**Figure 22:** Hillslope evolution with soil diffusion and chemical erosion. Varying climate with a “normal” climate defined by three hour storms of intensity one cm per hour and 104 storms per year and a “frequent rain” climate defined by three hour storms of intensity 0.25 cm per hour and 416 storms per year. Concave hillslope, 10,000 year simulation,  $D = 0.01 \text{ m}^2 \text{ yr}^{-1}$ ,  $c = 0.2$ , and  $R_{dis} = 2 \times 10^{-9} \text{ mol m}^{-2} \text{ s}^{-1}$ . Resultant chemical denudation rates when averaged over the planforms are approximately  $6 \times 10^{-4} \text{ m yr}^{-1}$  for both climates, with denudation ratios averaged over the planforms approximately 0.99 for both climates.

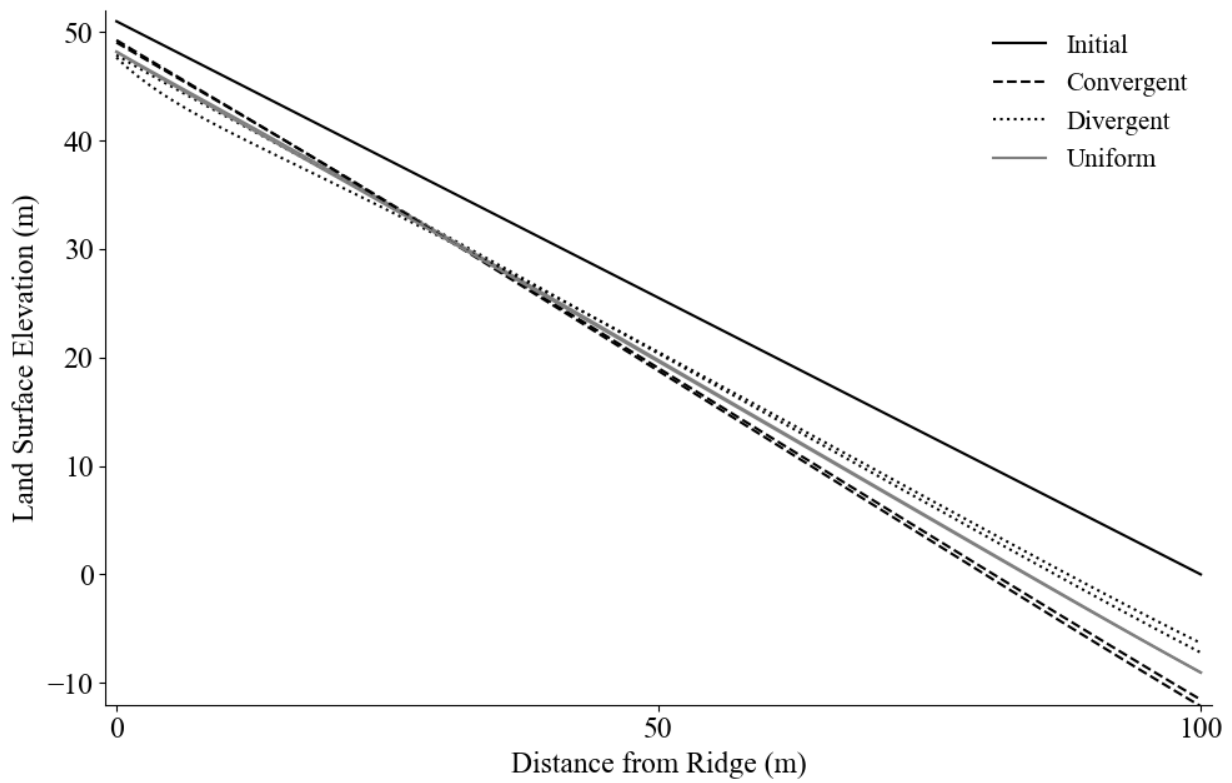


**Figure 23:** Hillslope evolution with soil diffusion and chemical erosion. Varying convergence rate from 0.2 to 0.35. Planar hillslope, 10,000 year simulation,  $D = 0.01 \text{ m}^2 \text{ s}^{-1}$ ,  $R_{dis} = 2 \times 10^{-9} \text{ mol m}^{-2} \text{ yr}^{-1}$ ,  $N = 0.009 \text{ m hr}^{-1}$ , 104 storms per year. Resultant chemical denudation rates for simulations with both convergence rates, when averaged over the planforms, are approximately  $5 \times 10^{-4} \text{ m yr}^{-1}$  with denudation ratios for the simulation with lower convergence rate 0.94 and with higher convergence rate 0.93.

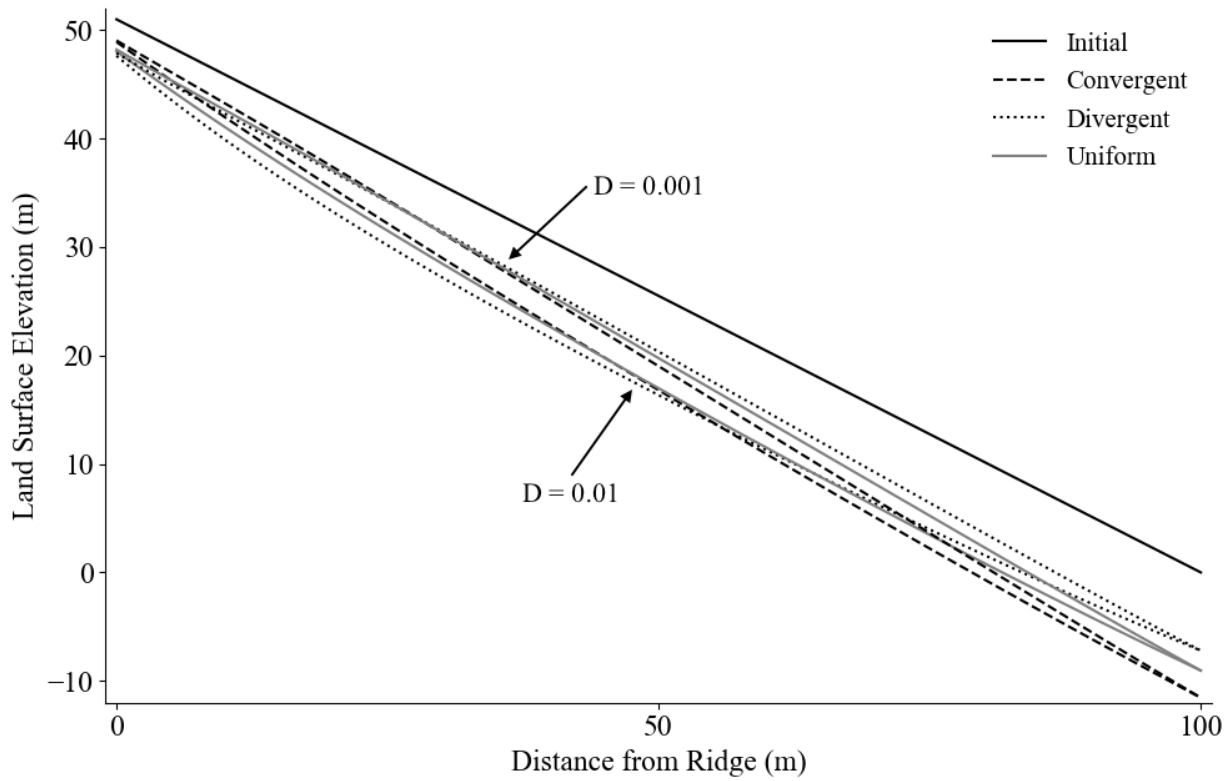


**Figure 24:** Hillslope evolution with soil diffusion and chemical erosion. Varying diffusivity from 0.01 to 0.001. Planar hillslope, 100,000 year simulation,  $R_{dis} = 2 \times 10^{-10} \text{ mol m}^{-2} \text{ s}^{-1}$ ,  $\dot{N} = 0.009 \text{ m hr}^{-1}$ , 104 storms per year. Resultant chemical denudation rates for both simulations, when averaged over the planforms, are approximately  $5 \times 10^{-5} \text{ m yr}^{-1}$  with denudation ratios, when averaged over the planforms, of approximately 0.65 for the simulation with  $D = 0.01 \text{ m}^2 \text{ yr}^{-1}$  and 0.94 for the simulation with  $D = 0.001$ .

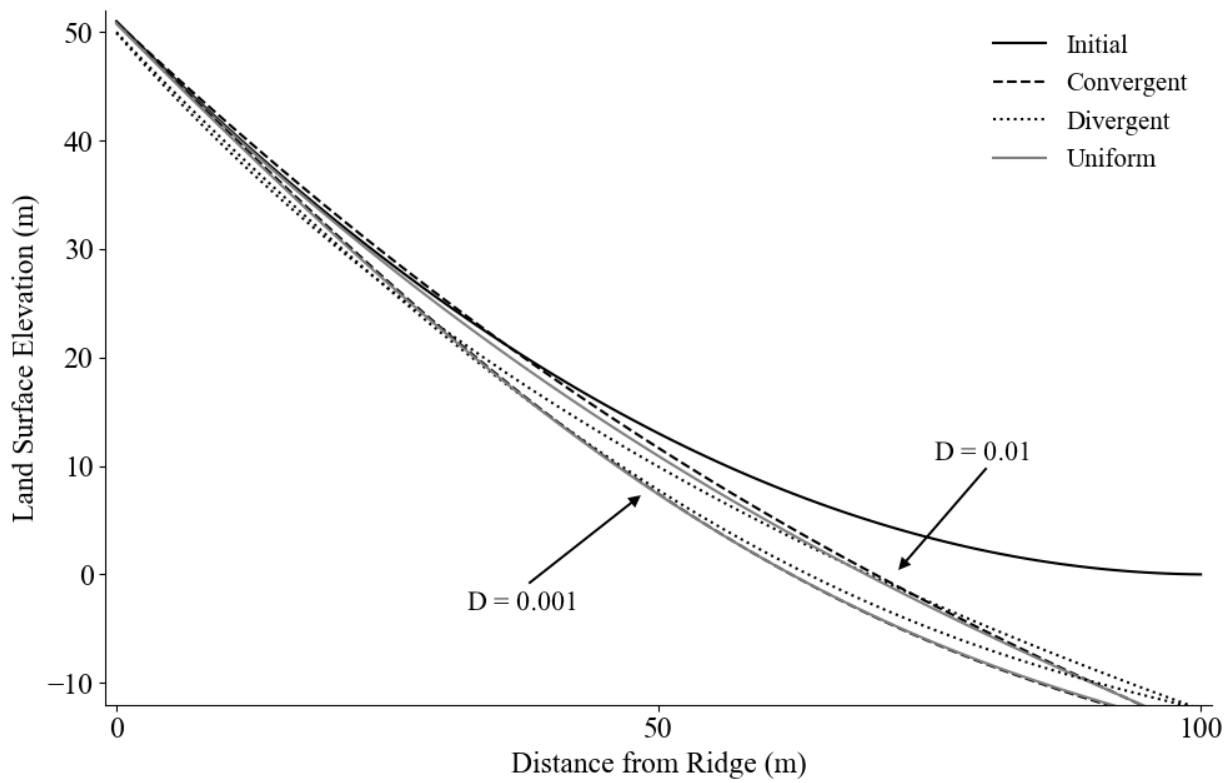


**Figure 25:** Hillslope evolution with soil diffusion and chemical erosion. Varying diffusivity from 0.01 to 0.001. Concave hillslope, 100,000 year simulation,  $R_{dis} = 2 \times 10^{-10} \text{ mol m}^{-2} \text{ s}^{-1}$ ,  $N = 0.009 \text{ m hr}^{-1}$ , 104 storms per year. Resultant chemical denudation rates for both simulations, when averaged over the planforms, are approximately  $6 \times 10^{-5} \text{ m yr}^{-1}$  with denudation ratios, when averaged over the planforms, of approximately 0.80 for the simulation with  $D = 0.01 \text{ m}^2 \text{ yr}^{-1}$  and 0.99 for the simulation with  $D = 0.001$ .